IEEE 2012 GLOBECOM
GLOBAL COMMUNICATIONS CONFERENCE, EXHIBITION & INDUSTRY FORUM

Issue 1
Monday, 3 December 2012

Welcome to IEEE GLOBECOM 2012 at Disneyland®!

General Chair
Hossein Eslambolchi

Executive Chair
Pierre Perra

Executive Vice Chair
Douglas N. Zuckerman

It is our great pleasure to welcome you to the IEEE Global Communications Conference (GLOBECOM 2012) on 3-7 December 2012 at the Disneyland® Hotel in Anaheim, California. The IEEE Communications Society's premier flagship conference will provide a unique opportunity to explore the leading areas of information and communications technology related to industry, academia, government, enterprise and other market segments from around the world. The relaxed setting of the conference, in the fabulous Disneyland® Hotel, will be especially conducive to networking with colleagues, friends, customers and vendors from around the world.

The theme of IEEE GLOBECOM 2012, "The Magic of Global Connectivity," specifically matches the conference location, setting the focus on leading edge coverage of communications with and across all parts of our planet and into deep space. IEEE GLOBECOM 2012 at the Disneyland® Hotel, through its extensive coverage of the field from various angles, will result in an unforgettable and highly valuable experience. This important conference will offer you a wide range of technical, educational and professional opportunities, featuring, but not limited to:

Technical Program

Technical Symposia – providing numerous technical sessions with papers presenting the latest technical advances through peer-reviewed paper sessions

Tutorials – offering education for keeping up with new and emerging topics essential to current engineering and technology environment

Workshops – with specialized focus on the latest breakthroughs in information and communications technology in an environment that encourages discussion and debate

Industry Forum and Exhibition

Communications Forum and Exhibition Keynote Speakers – visionaries such as **Vinton Cerf**, **Henry Samueli**, **Krish Prabhu** and **Stephen Alexander** will challenge you in exciting new technology and practice

Executive Forum – hear our industry's top leaders sharing their visions of the future for the Communications industry

Industry Tutorials, Special Topics and Congress - including Social Networking & Digital Games, IPv6 focus, IEEE Cloud Computing Initiative, Green Communication Standards and Industry-University Education Collaboration

Business Forums – featuring exciting panel sessions on enterprise networking, access, capital resources and intellectual property business models

Exhibition – patron vendors showcasing their latest technologies and applications, as well as opportunities for "sales on the spot"

Professional Development

Career Forum – of special interest to students, entrepreneurs and anyone who takes an interest in their career development and capital investment

Special Interest Groups – including IEEE Graduates of the Last Decade (GOLD) and IEEE Women in Engineering (WIE)

Lightning Talks and Student Contests – aimed at providing an opportunity for students to demonstrate their skills through demos or other activities

We are doing our best to make your participation at IEEE GLOBECOM 2012 at the Disneyland® Hotel one of the most valuable and memorable experiences of your life from both professional and personal perspectives.

We look forward to meeting you during the conference.

Hossein, Pierre and Doug

TABLE OF CONTENTS

PAPER SMART CONFERENCE

IEEE GLOBECOM 2012 is a paper smart conference.
There will be no printed final programs distributed onsite at the conference.
The final program is available at **http://www.ieee-globecom.org/2012/finalprogram.html** in PDF and FlipBook searchable formats.

The conference venues, Disneyland® Hotel and Grand Californian Hotel, will both be equipped with wireless access points.
There will also be computer stations available in the registration and exhibit hall areas for those
who may need to view the conference program.

The only printed material is the Program Guide found in your badge holder.

PROGRAM SPOTLIGHT

CONTEST

IEEE GLOBECOM 2012 SARACEN Contest
Win a Tablet!

SARACEN

Competition
A first at IEEE GLOBECOM 2012, the SARACEN project, in parallel with its demos, is running a video competition to publicize and document the conference. The competition is open to all attendees. Simply use your camera or mobile phone to produce and upload a video to the SARACEN platform on "What is IEEE GLOBECOM." Upload content and complete a questionnaire on by Wednesday, 5 December 2012 to enter with a chance of winning. The goal is to tell everyone what IEEE GLOBECOM is all about. The winner of the contest will be awarded with a tablet at the Lightning Talks session in North Ballroom A on Thursday, 6 December 2012, which is the last session of the Industry Forums.

What is SARACEN?
Visit the SARACEN booth at the Exhibit Floor in Central Ballroom. Saracen is an EU funded research project, which has produced a peer to peer video streaming client, enhanced by Social Networking capabilities, and participants are able to use the platform to upload, view, and comment on, or rate videos.

How to participate
1. To take part in the contest you need to register on the platform. Just visit the SARACEN booth in the Industry Exhibition, to find out more and register. Additional information can be found on the SARACEN website, **http://www.saracen-p2p.eu/content/contest-ieee-globecom-2012**.
2. Once you have registered your account, download the SARACEN client to your PC.
3. Make a short film on "What is IEEE GLOBECOM." Only submit videos that you have taken at IEEE GLOBECOM 2012 (no copyrighted material without permission).
4. Upload your film to the Saracen platform using the Saracen client.
5. Tag the film IEEE GLOBECOM 2012, to characterize the video.
6. Search for, watch, comment on, tag and rate other IEEE GLOBECOM video entries
7. Last step (optional): give us your feedback – tell us what you think of the platform and client using the feedback form on the SARACEN website, **http://www.saracen-p2p.eu/content/questionnaire**, or complete a printed form at the SARACEN booth.

Contest Rules Reinforced
All entries should adhere to these common rules to protect privacy and anonymity, and to avoid any implications that could jeopardize engineering professionalism with the uploaded material.
1. SARACEN/IEEE GLOBECOM 2012 cannot return any uploaded videos
2. No racially, sexually, religiously offensive material
3. No intrusion of personal privacy
4. English only videos
5. Participants should conduct with respectable ethics and IEEE professional standards

Contact at the Exhibition Hall: Charalampos Patrikakis, email: **bpatr@telecom.ntua.gr**

PROGRAM SPOTLIGHT

IEEE CLOUD COMPUTING CONGRESS at IEEE GLOBECOM 2012

The IEEE Cloud Computing Congress being held in North America is part of an overall presence of the IEEE Cloud Computing Initiative (see **http://cloudcomputing.ieee.org/**) at IEEE GLOBECOM 2012. The congress consists of a tutorial, executive forum, several Industry Forum and Exposition (IF&E) sessions and a technical workshop. The IEEE Cloud Computing Initiative (CCI), launched in April 2011 and significantly funded in 2012, intends to help accelerate the development and use of cloud computing technologies and help advance the understanding and use of the cloud computing paradigm by coordinating IEEE cloud computing conferences, publications, standards, educational, and regional activities. The IEEE Cloud Computing Web Portal provides members of the technical community as well as the general public a convenient, centralized gateway to news and information about cloud computing and the many activities organized and led by the IEEE CCI.

Cloud computing already has widespread impact across how we access today's applications, resources, and data. Many issues around cloud computing need to be addressed, including, but not limited to, security, reliability, architecture, and economics. During this congress, special attention will be given to the role of standards as an enabler of cloud interoperability, the business value of cloud computing, big data and the cloud, the impact of cloud computing on network infrastructures, and user experiences with the cloud computing paradigm.

Tutorial:

Programmable Cloud Computing and Networking
Masum Hasan and **Edgar Magana**, Cisco, USA

Executive Forum:

IT Transformation: Clouds, Security, Mobility and Computing
Flavio Bonomi, VP & Head, Advanced Architecture and Research Organization, Cisco Systems, USA
Hamid Ahmadi, VP & Head, Advanced System Engineering Lab, Samsung Information Technology America, USA
Steven D. Gray, CTO, CSR, USA
Patricia Florissi, CTO RMSG, EMC, USA

Industry Forum:

Cloud Computing Interoperability
Doug Zuckerman, Senior Scientist, Applied Communication Sciences, USA, IEEE Fellow
Introduction: IEEE Cloud Computing Initiative (CCI) and Cloud Interoperability
Joe Weinman, Senior Vice President, Telx, USA
The Insights of Cloudonomics
Jeffrey Voas, Computer Scientist, National Institute of Standards and Technology, USA, IEEE Fellow
The Difficulties in Cloud Security and Cloud Testing
Jeffrey S. Chase, Professor, Department of Computer Science, Duke University, USA
Community Multi-Clouds: Perspectives from NSF's GENI Project
David G. Belanger, Chief Scientist & Fellow, AT&T Labs, USA
Big Data and the Cloud

Industry Forum:

Cloud Computing Industry Perspectives
Mark Karol, IEEE Fellow, USA
Cloud Computing, Communications, and Networking: Perspectives and Issues
Douglas Freimuth, Senior Technical Staff Member, IBM TJ Watson Research Center, USA
Dynamic Networks and the Cloud
James Prendergast, Executive Director & COO, IEEE, USA
Leveraging the Cloud for IEEE's Products & Services
Wu Chou, Vice President & Chief IT Scientist, Head of Huawei IT Lab, Huawei USA, IEEE Fellow
Cloud Computing for Communication
Richard Lau, Chief Scientist & Fellow, Applied Communication Sciences, USA
Cloud Priority Service
Shueng-Han Gary Chan, Associate Professor, HKUST, Hong Kong
Deployment of an Advanced Streaming Cloud for Multimedia Broadcasting

Technical Workshop:

Management and Security Technologies for Cloud Computing 2012
Raouf Boutaba, University of Waterloo, Canada
Panagiotis Rizomiliotis, University of the Aegean, Greece
Charalabos Skianis, University of the Aegean, Greece
Jianying Zhou, Institute for Infocomm Research, Singapore

See the final program,
http://www.ieee-globecom.org/2012/finalprogram.html,
for times, dates and room locations.

EVENTS OF THE DAY

08:00 – 18:00

Workshops

08:00 – 15:30
W7: Optical Wireless Communications (OWC) / Castle B

08:00 – 18:00
W3: Workshop on Radar and Sonar Networks (RSN)
/ North Exhibit Hall F

08:10 – 18:00
W1: Heterogeneous and Small Cell Networks (HetSNets) / Castle C

08:30 – 17:00
W10: Management of Emerging Networks and Services (MENS) / Monorail A/B

08:30 – 17:20
W4: Emerging Technologies for LTE-Advanced and Beyond-4G (LTE-B4G)
/ North Exhibit Hall D/E

08:30 – 17:30
W8: Smart Grid Communications: Design for Performance (SGComm) / North Exhibit Hall I

08:30 – 18:00
W5: Heterogeneous, Multi-hop, Wireless and Mobile Networks (Heterwmn)
/ North Exhibit Hall G/H
W9: Cloud Base-station and Large-scale Cooperative Communications (CACAO)
/ North Exhibit Hall Room J

08:40 – 18:00
W11: Mobility Management in the Networks of the Future World (MobiWorld)
/ Monorail C

08:50 – 18:00
W6: Multicell Cooperation (MuCo) / Castle A

09:00 – 17:15
W2: Broadband Wireless Access (BWA)
/ North Exhibit Hall B/C

09:00 – 12:00

Tutorials

IF1: Small Cell & HetNet Deployment / North Ballroom A
IF2: Digital Games for "People" Networking / North Ballroom B
T1: Small Cell Wireless Networks / South Ballroom A/B
T2: Mobile-Station and Base-Station Cooperation / Magic Kingdom Ballroom 1/4
T3: Gigabit Wireless LAN
/ Magic Kingdom Ballroom 2/3

12:00 – 14:00
Lunch (Workshop and Tutorials (AM) Only) / Center Ballroom

14:00 – 17:00

Tutorials

IF3: Programmable Cloud Computing & Networking
/ North Ballroom A
IF4: Internet as a New Paradigm / North Ballroom B
IF5: Software Testing in the Network Environment
/ North Exhibit Hall A
T4: Content Delivery Acceleration / South Ballroom A/B
T5: Wireless Cognitive Radio Network / Magic Kingdom Ballroom 1/4
T6: M2M in Smart Grid & Smart Cities / Magic Kingdom Ballroom 2/3

18:00 – 19:00
First Time Attendee Reception (By Invitation Only)
/ Sleeping Beauty Pavilion

19:00 – 21:30
Welcome & EXPO Opening / South Exhibit Hall

PROGRAM UPDATES

The following are updates to the program guide found in your badge holder. These updates appear in the online final program.

Monday, 3 December 2012

T2: Mobile-Station and Base-Station Cooperation
from 09:00 – 12:00 will now be held in Magic Kingdom Ballroom 1/4.
T3: Gigabit Wireless LAN
from 09:00 – 12:00 will now be held in Magic Kingdom Ballroom 2/3.
T5: Wireless Cognitive Radio Network
from 14:00 – 17:00 will now be held in Magic Kingdom Ballroom 1/4.
T6: M2M in Smart Grid & Smart Cities
from 14:00 – 17:00 will now be held in Magic Kingdom Ballroom 2/3.

Tuesday, 4 December 2012

IF8: M2M/IoT: What are the Futures in Communication?
from 10:00 – 12:00 will now be held in North Ballroom A.
IF11: Green Communication & Computing
from 13:45 – 15:30 will now be held in North Ballroom A.
IF14: The Grand Debate: Internet vs. Telecommunications
from 16:00 – 18:00 will now be held in North Ballroom A.

Wednesday, 5 December 2012

IF17: Next Generation Cellular & Satellite Communication I
from 10:00 – 12:00 will now be held in North Ballroom A.
IF18: Next Generation Cellular & Satellite Communication II
from 13:30 – 15:30 will now be held in North Ballroom A.
IF22: Education Forum
from 16:00 – 18:00 will now be held in North Ballroom A.

Thursday, 6 December 2012

IF25: Cable Industry Access Technology
from 16:00 – 18:00 will now be held in North Ballroom A.
IF28: Optical Wireless Access
from 13:30 – 15:30 will now be held in North Ballroom A.
IF23: Lightning Talks
from 16:00 – 18:00 will now be held in North Ballroom A.

Friday, 7 December 2012

T9: Opportunistic Communication
from 09:00 – 12:00 will now be held in Magic Kingdom Ballroom 1/4.
T12: Cooperative Spectrum Sensing
from 14:00 – 17:00 will now be held in Magic Kingdom Ballroom 1/4.

DINING AND ENTERTAINMENT
in the Downtown Disney® District (courtesy of Disney®)

Looking for ways to decompress and unwind after a long day of meetings? At the Disneyland® Resort, we offer fun ways to spark imaginations outside the boardroom as well. Welcome to the Downtown Disney® District, conveniently situated between our two theme parks and a short walk from our three hotels. With live music and a unique variety of restaurants and shops to explore, one can't help but be happy and in high spirits in this relaxed, inspired atmosphere.

Dining

To make reservations, call Disney® Dining at +1 (714) 781.3463.

Catal Restaurant

http://disneyland.disney.go.com/downtown-disney/catal-restaurant/
Location: Downtown Disney® District
Cuisine: Healthy Selections, Mediterranean, Steak, Vegetarian
Experience divine dining at Catal Restaurant, from a casual bite to an exquisite multi-course Mediterranean feast. Menu items include grilled seafood, poultry, vegetables, pastas and more. Enjoy the romantic rustic atmosphere inside or the panoramic view on the patio.

The Coffee House

Location: Disneyland® Hotel
Cuisine: American
Get going with a variety of quick breakfast items including muffins, biscotti, bagels, yogurt and coffee. This convenient coffee shop is a great way to begin your day.

Earl of Sandwich

http://disneyland.disney.go.com/downtown-disney/earl-of-sandwich/
Location: Downtown Disney® District
Cuisine: American, Healthy Selections, Vegetarian
With connections to the 18th-century inventor of the sandwich and 250 years of experience of creating quick and hearty meals, this casual restaurant raises sandwich making to an art with fresh-baked bread, fine ingredients and such signature items as The Original 1762.

ESPN Zone

http://disneyland.disney.go.com/downtown-disney/espn-zone-restaurant/
Location: Downtown Disney® District
Cuisine: American, Healthy Selections, Vegetarian
Feast on generous portions of expertly prepared American food like chops, steaks, burgers and salmon — all grilled to perfection. The food is only part of the total ESPN entertainment, shopping and dining experience.

Hearthstone Lounge

Location: Disney's Grand Californian Hotel & Spa
Cuisine: American
Gather with good friends around the cozy fireplace in this lodge-like lounge and sip on a drink from the full bar. In the morning, enjoy a continental breakfast with fresh bakery goods, specialty coffees and a sweeping view.

House of Blues Restaurant

http://disneyland.disney.go.com/downtown-disney/house-of-blues-restaurant/
Location: Downtown Disney® District
Cuisine: American, Cajun-Creole, Steak
Dine on cuisine inspired by the South as renowned musical acts light up the stage for your entertainment. The menu features down home temptations like Voodoo Shrimp and Cajun-Creole seafood jambalaya, along with sizzling steaks, burgers and ribs.

La Brea Bakery Café

http://disneyland.disney.go.com/downtown-disney/la-brea-bakery-cafe/
Location: Downtown Disney® District
Cuisine: American, Californian
Enjoy the relaxing confines of the delightful outdoor patio while selecting from a menu featuring gourmet sandwiches, pastries and other unique rustic choices. Open for breakfast, lunch and dinner, this celebrated family bakery is famous for "bringing bread to life."

Napa Rose

http://disneyland.disney.go.com/grand-californian-hotel/napa-rose/
Location: Disney's Grand Californian Hotel & Spa
Cuisine: American, Californian, Healthy Selections, Vegetarian
Enjoy a glass of wine from the award-winning collection with exquisite seasonal creations for a fresh culinary experience that rivals fine-dining establishments anywhere in the world. Napa Rose was named the Most Popular Restaurant in the 2008 Zagat Survey for Orange County.

Naples Ristorante e Pizzeria

http://disneyland.disney.go.com/downtown-disney/naples-ristorante-e-pizzeria/
Location: Downtown Disney® District
Cuisine: Healthy Selections, Italian, Vegetarian
Savor delectable thin-crust pizzas and delicious pastas from the bustling chefs in the open kitchen. Watch the cooks twirl pizzas and bake them to perfection in wood-burning ovens. Luscious salads and other authentic Italian entrees are also served.

Napolini

Location: Downtown Disney® District
Cuisine: American, Healthy Selections, Italian, Vegetarian\For great-tasting Italian food to go, nothing tops Napolini, a gourmet Italian deli. Authentic Italian fare includes fresh salads, delicious pastas, pizza and mouthwatering paninis.

Rainforest Cafe

http://disneyland.disney.go.com/downtown-disney/rainforest-cafe/
Location: Downtown Disney® District
Cuisine: American, Healthy Selections, Steak
Explore a tropical rainforest — complete with waterfalls, rain showers, live parrots, animated apes and all the sounds of a real jungle — at this unique dining adventure. Savor generous portions of food from around the world under a shimmering fiber-optic starscape.

Ralph Brennan's Jazz Kitchen

http://disneyland.disney.go.com/downtown-disney/ralph-brennans-jazz-kitchen/
Location: Downtown Disney® District
Cuisine: Cajun-Creole, Steak
Sample the spiciness of Cajun cuisine with gumbo, Gulf seafood, po' boy sandwiches and decadent desserts. As part of a total entertainment and dining experience, the music never stops and Bourbon Street's legendary party atmosphere pulsates to life.

DINING AND ENTERTAINMENT
in the Downtown Disney® District (courtesy of Disney®)

Steakhouse 55
http://disneyland.disney.go.com/disneyland-hotel/steakhouse-55/
Location: Disneyland® Hotel
Cuisine: American, Healthy Selections, Steak, Vegetarian
Indulge in an elegant dining experience with unparalleled service and a menu featuring an award-winning selection of prime steaks, chops and seafood. Savor certified Angus beef cuts and take advantage of a premium wine list. Breakfast is available.

Storytellers Cafe
http://disneyland.disney.go.com/grand-californian-hotel/storytellers-cafe/
Location: Disney's Grand Californian Hotel & Spa
Cuisine: American, Healthy Selections, Vegetarian
Hearty home-style favorites like wood-fired pizzas, fresh salads, grilled sandwiches and scrumptious fish highlight the rustic menu, while the storytelling tradition is saluted in beautiful period murals depicting tall tales from early California.

Surfside Lounge
Location: Disney's Paradise Pier Hotel
Cuisine Type: American
Relax with a cocktail or glass of wine at this laidback lounge located adjacent to Disney's PCH Grill in the lobby of Disney's Paradise Pier Hotel.

Tangaroa Terrace – Casual Island Dining
http://disneyland.disney.go.com/disneyland-hotel/tangaroa-terrace/
Location: Disneyland® Hotel
Cuisine: American, Healthy Selections
Inspired by Adventureland at Disney Parks worldwide, this locale includes tiki torches and tropical music. Specialties include French toast with warm banana-caramel sauce for breakfast and Hawaiian Angus burgers for lunch. Each evening, savor an Island Plate Dinner Special such as miso-crusted salmon.

Taqueria at Tortilla Jo's
Location: Downtown Disney® District
Cuisine: Healthy Selections, Mexican, Vegetarian
Mouth-watering traditional Mexican dishes and magnificent margaritas make Tortilla Jo's the perfect gathering place for fun and drinks. The outdoor taqueria lets you create your own custom-built tacos, nachos and burritos while sipping on house-made aguas frescas.

Tortilla Jo's
http://disneyland.disney.go.com/downtown-disney/tortilla-jos/
Location: Downtown Disney® District
Cuisine: Healthy Selections, Mexican, Vegetarian
Indulge in a mixture of Mexican culinary traditions including taquitos, "drowned" nachos and Camarones Diablos with spicy shrimp and cracklings. Tortilla Jo's also features live mariachis, an outdoor dining cantina, a hand-made tortilla station and happy hour every weekday!

Trader Sam's – Enchanted Tiki Bar
http://disneyland.disney.go.com/disneyland-hotel/trader-sams/
Location: Disneyland® Hotel
Cuisine: American
Escape to this unique, interactive lounge experience with a bit of Disney magic, adjacent to Tangaroa Terrace – Casual Island Dining. Set a course for this Jungle Cruise-inspired hideaway for tropical cocktails, juices and an ambrosial bar menu – fit for the gods!

Uva Bar
Location: Downtown Disney® District
Cuisine: Mediterranean
Savor Cal-Mediterranean favorites and sip on refreshing craft beers and signature cocktails at this Downtown Disney al fresco destination. Bar snacks, crisp salads and decadent burgers seared a la plancha provide a taste of Spain adjacent to Disneyland Park. Make sure to save room for the homemade ice cream sandwiches, floats and shakes.

ENTERTAINMENT

House of Blues Stage
http://disneyland.disney.go.com/downtown-disney/house-of-blues-stage/
Location: Downtown Disney® District
Take your place in front of the stage where legends are made! You won't be able to stop dancing. See world-famous performers, live and in person, as well as the best up-and-coming talent from around the region.

Ralph Brennan's Jazz Kitchen – Flambeaux's Jazz Club
http://disneyland.disney.go.com/downtown-disney/ralph-brennans-jazz-kitchen-flambeauxs-jazz-club/
Location: Downtown Disney® District
Listen to the best of live jazz and discover the true taste of New Orleans. With the aroma of spicy cooking, enjoy the sounds of even spicier music! In the atmosphere of Bourbon Street the jazz goes on, from straight-ahead to Dixieland.

ESPN Zone Sports Arena
http://disneyland.disney.go.com/downtown-disney/espn-zone-sports-arena/
Location: Downtown Disney® District
Over 120 HDTV's fill this sports fan's paradise! Chow down on a menu fit for a world champion. Starters include wings, sliders and pizza. Feast on generous portions of steaks, burgers and salmon — all grilled to perfection. Then bring your skills to the Sports Arena Arcade for 10,000 square feet of action-packed sports gaming.

IEEE GLOBECOM 2012
BEST PAPERS

The conference best papers will be announced at the end of the Keynote and Opening Session on Tuesday, 4 December. These papers will be included in this section daily. On the following pages, the first 3 of 15 papers featured are from Symposia on Selected Areas of Communications, Communication Theory and Cognitive Radio and Networks.

Proactive Channel Gain Estimation for Coexistence between Cognitive and Primary Users

Lin Zhang⋆, Guodong Zhao♯⋆, Gang Wu⋆, and Zhi Chen⋆
⋆ NCL, University of Electronic Science and Technology of China, Chengdu, China
♯ ECE, The Hong Kong University of Science and Technology, Hong Kong

***Abstract*— In cognitive radio systems, the channel gains between primary users (PUs) and cognitive users (CUs) and that between PUs are critical for the coexistence of CUs and PUs. In this paper, we propose a proactive channel gain estimation approach by using the received primary signal for probing, which obtains both kinds of channel gains without information exchange between CUs and PUs. In average, the probing in our proactive approach does not introduce interference to PUs while conventional ones usually do. Simulation results show that the relative estimation errors of the proposed approach are below 0.02 with a proper CU location, where the channels suffer path loss and shadowing, and their gains range from about -120 dB to about -50 dB.**

***Index Terms*— Cognitive radio, channel gain estimation, proactive sensing, probing, interference-free.**

I. Introduction

Cognitive radio (CR) is a promising technique to deal with spectrum shortage issue in future wireless communications, where *cognitive users* (CUs), also called secondary users, access the frequency bands allocated to existing users, also called *primary users* (PUs), if the interference generated by CUs is ignorable [1]. Generally, CUs access the frequency bands in two ways, *opportunistic spectrum access* (OSA) and *spectrum sharing* (SS) [2]. In OSA, CUs determine whether to access a certain frequency band by detecting the PU's working status and only access the band when PU is detected to be inactive. Once the PU is detected to be active, CUs have to free the band as soon as possible [3].

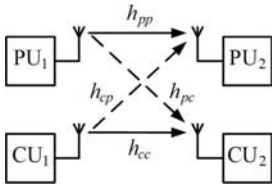

Fig. 1. Coexistence between CUs and PUs (Spectrum sharing, SS).

In SS, CUs and PUs are able to simultaneously access a common frequency band as shown in Fig. 1, provided that the interference power at PU_2 generated by CU_1 is lower than a tolerable threshold. From the perspective of information theory [4]-[6], significant CR capacity can be achieved by SS on condition that CUs are aware of *channel state information* (CSI), e.g., h_{cc}, h_{pc}, h_{cp}, and h_{pp} in Fig. 1. In practice, it is easy to obtain the CSI of Channels h_{cc} and h_{pc} by CU_1 directly. However, it is very challenging to obtain the CSI of Channels h_{cp} and h_{pp} since PUs may be unwilling to cooperate or cannot cooperate with CUs. As a result, CSI estimation becomes the bottleneck for implementing SS, which limits the applications of CR.

To deal with the issue without information exchange between CUs and PUs, we will propose an approach to estimate the channel gain* from CU_1 to PU_2 and that between the two PUs, i.e., h_{cp}^2 and h_{pp}^2, respectively. Basically, our approach is motivated by the recent probing sensing technique in CR [7], where a CU performs spectrum sensing in a proactive way. As shown in Fig. 1, CU_1 first sends a probing signal to trigger the *closed-loop power control* (CLPC) in PUs, which has been widely used in existing wireless systems. Under the power control, PU_1 will adjust its transmission power as a response to CU_1 probing signal, which is related to the gains of Channels h_{cp} and h_{pp}. Thus, by observing the response, CU_1 is able to obtain valuable information associated with the channel gain from CU_1 to PU_2 as in Fig. 1. Based on the principle, a proactive spectrum sensing method has been proposed in [7] to detect PU_2. Two active learning methods have been introduced in [2] and [8] to obtain the channel gain from CU_1 to PU_2. However, as indicated in [7], the probing signal may cause temporal interference to PUs, which may be illegal. In [2], the proposed active learning method can only obtain the ratio between the channel gain h_{cp}^2 and the noise power of PU_2, i.e., $h_{cp}^2/\sigma_{\mathrm{PU}_2}^2$. In [8], even though the channel gain h_{cp}^2 can be obtained, the method requires CU_1 to decode the control signal from the PU's feedback. This involves cooperation between CUs and PUs, which may be infeasible. To the best of our knowledge, there is no effective way to obtain the channel gain between CU to PU and even that between PUs, which is crucial for realizing SS in CR.

In the proposed method of this paper, the received PU_1

The corresponding author is Guodong Zhao and the contact email is gdngzhao@gmail.com. This paper is partially supported by the National Basic Research Program of China under Grant 2012CB316003, the National High-Tech R&D Program of China under Grant 2011AA01A105, and the National Natural Science of Foundation of China under Grant 60972029.

*When CUs and PUs are with no cooperation, it is hard to estimate complex channel coefficients since it requires channel estimation. This involves synchronizing primary signal, which is impractical for heterogeneous systems, i.e., cognitive and primary systems. Thus, we study the estimation of channel gains.

signal is used as the probing signal, thus the interference to PU_2 due to the probing can be eliminated. Meanwhile, by using of the received PU_1 signal for probing, CU_1 may not only estimate the channel gain from CU_1 to PU_2, i.e., h_{cp}^2, but also obtain the channel gain between the two PUs, i.e., h_{pp}^2.

The rest of this paper is organized as follows. In Section II, we describe the system model. In Sections III and IV, we develop the the proposed estimation method and provide the simulation results. Finally, Section V concludes the paper.

II. System Model

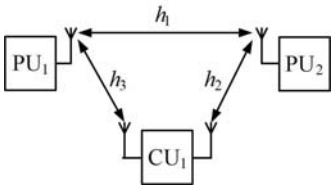

Fig. 2. System model of proactive channel gain estimation.

As shown in Fig. 2, two PUs and one CU are considered to develop our algorithm, where the two PUs are working in a certain frequency band in *time division duplex* (TDD) mode and communicate with each other through Channel 1, i.e., h_1. CU_1 intends to access the same frequency band as the PUs for CR commutation. Here, CU_1 has to control its power to limit the interference to PU_1 and PU_2 through Channels 3 and 2, i.e., h_3 and h_2, respectively.

When PU_1 transmits a signal[†] to PU_2, the received signal at PU_2 can be expressed as

$$y_{21}(k) = \sqrt{p}h_1 x(k) + n_2(k), \tag{1}$$

where p represents the power of the transmitted signal $x(k)$ with normalized power, k is the index of samples, h_1 denotes the channel coefficient between PU_1 and PU_2, and $n_2(k)$ is the *additive white Gaussian noise* (AWGN) at PU_2 with zero mean and variance σ^2, i.e., $n_2(k) \backsim \mathcal{N}(0, \sigma^2)$.

Let p_{I_2} denote the power of the transmitted interference from CU_1, then the corresponding signal-to-interference-plus-noise ratio (SINR) at PU_2 can be given by

$$\gamma = \frac{ph_1^2}{p_{I_2}h_2^2 + p_{n_2}}, \tag{2}$$

where p_{n_2} represents the noise power at PU_2.

Assuming that the PUs require a constant data rate, then CLPC between them is applied, under which PUs are able to adjust their transmission power to compensate the SINR loss. Let γ_{T_2} be the targeted SINR of PU_2, the transmission power of PU_1 can be obtained by

$$p_1 = \frac{\gamma_{T_2}(p_{I_2}h_2^2 + p_{n_2})}{h_1^2}. \tag{3}$$

[†]The real signals and real channel coefficients are considered in this paper to simplify our derivation. The developed approach is also applicable for complex signals.

Usually, quantified information is used for CLPC feedback in practical wireless systems. To facilitate the analysis, perfect feedback is assumed in CLPC, i.e., no quantization and transmission errors.

When PU_2 transmits a signal back to PU_1, the transmission power of PU_2 will be

$$p_2 = \frac{\gamma_{T_1}(p_{I_1}h_3^2 + p_{n_1})}{h_1^2}, \tag{4}$$

where p_{I_1} and p_{n_1} indicate the interference power and noise power at PU_1, γ_{T_1} denotes the targeted SINR at PU_1 for the constant data rate. To simplify our derivation, we consider that the required data rates of the two PUs are identical, then $\gamma_{T_1} = \gamma_{T_2} = \gamma_T$.

In practice, when the corporation between CU_1 and the PUs does not exist, CU_1 can only measure the power adjustment of PUs. Let γ_{r_1} and γ_{r_2} denote the observed *signal-to-noise ratio* (SNR)[‡] when PU_1 transmits a signal to PU_2 and that when PU_2 transmits a signal back to PU_1. It is assumed that all the channels are static and all the noise are *independent identical distributed* (IID) AWGN variables with zero mean variance σ^2. Under these assumptions, we have

$$\gamma_{r_1} = \frac{p_1 h_3^2}{p_{n_r}} \quad \text{and} \quad \gamma_{r_2} = \frac{p_2 h_2^2}{p_{n_r}} \tag{5}$$

where p_{n_r} represents the power of AWGN at CU_1, p_1 and p_2 denote the instantaneous transmission power of PU_1 and PU_2, respectively.

In order to realize the coexistence between CU_1 and the PUs, CU_1 is required to obtain the channel gains of h_1, h_2, and h_3, i.e., h_1^2, h_2^2, and h_3^2. Otherwise, CU_1 may overlook cognitive transmission opportunities.

III. Proactive Channel Gain Estimation

In this section, we will first introduce the principle of our proactive channel gain estimation, then develop the probing process and design the estimator. Finally, we will discuss the relationship between our approach and a conventional one.

A. Principle

As introduced before, the power of a PU transmitter, say PU_1, under CLPC is adjusted according to the SNR[§] at a PU receiver, say PU_2. Specifically, if SNR at PU_2 decreases, the corresponding transmitter PU_1 on the other side will increase its transmission power to compensate the SNR loss. If the SNR at PU_2 increases, PU_1 will reduce the power to maintain the constant data rate. On the other hand, the SNR at PU_2 is affected by Channels 1, 2, and 3. Then the power variation of PU_1 is a function of h_1^2, h_2^2, and h_3^2, i.e., the gains of Channels 1, 2, and 3. Therefore, CU_1 may obtain the estimations of h_1^2,

[‡]In this paper, both SNR and SINR are denoted as $\gamma_{\Phi}^{\varsigma}$, where ς and Φ are the up and low subscripts of γ.

[§]Here, SNR is used in Sections III-A and -B since the received PU signal is applied for probing in our approach and it does not introduce interference, while SINR is used in Section III-C since a generated jamming signal is applied for probing in conventional methods and they cause interference to PUs.

h_2^2, and h_3^2 by observing the power variations of the PUs, which are triggered by CU_1's probing signal.

To obtain these estimations, we propose a proactive channel gain estimation algorithm, where CU_1 receives, amplifies, and forwards the received primary signal to trigger PUs' CLPC by enhancing the SNR at PU receivers. Based on the algorithm, CU_1 can not only obtain the channel gains of h_1, h_2, and h_3 without interference to PUs but also provides some diversity for PUs temporarily.

Here, each PU is equipped with one antenna for reception and transmission while CU_1 is equipped with two antennas, one for reception and the other for transmission. Furthermore, CU_1 is assumed to adopt perfect echo cancelation to avoid self-interference when receiving and transmitting signals simultaneously at the same frequency band. The impact on the proposed algorithm due to imperfect echo cancelation is beyond the scope of this paper.

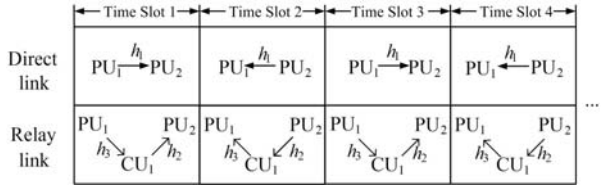

Fig. 3. Time slot flow for proactive channel gain estimation.

Fig. 3 illustrates the time slot flow of our algorithm. PU_1 and PU_2 transmit signals alternately, i.e., PU_1 transmits signals to PU_2 in odd time slots while PU_2 transmits signals to PU_1 in even time slots. Here, we consider four time slots to develop our algorithm. In the time slot 1, PU_1 transmits a primary signal to PU_2 with Power p. At the same time, CU_1 obtains the PU_1 signal with its receiving antenna through h_3, amplifies the signal with the amplitude gain G_2, and transmits the amplified signal to PU_2 through h_2. The time delays of reception, amplification, and transmission are assumed to be ignorable, which is reasonable in practice[¶]. At PU_2, the corresponding received signal consists of two parts, one from PU_1 through direct link and the other from CU_1 through relay link[‖]. As a result, the SNR is enhanced by CU_1, which triggers PUs' CLPC. Upon receiving a control signal from PU_2, PU_1 adjusts its transmission power to p_1 for the transmission in the time slot 3.

For the transmission from PU_1 to PU_2, CU_1 is able to obtain the SNR γ_{r_1} and the updated SNR $\gamma_{r_1}^{'}$ of PU_1 signals in the time slot 1 and 3, respectively. Similarly, in the reverse transmission, where PU_2 transmits a primary signal to PU_1, CU_1 can obtain the SNR γ_{r_2} and the updated SNR $\gamma_{r_2}^{'}$ of PU_2 signals in the time slots 2 and 4, respectively. Based on the observed SNRs, CU_1 obtains the estimations of h_1^2, h_2^2, and h_3^2 .

[¶]This can be looked as a wireless repeater, which has been widely used in 2G and 3G system. It requires to isolate transmitting and receiving antennas to cancel self-interference.

[‖]We use the notion relay link since CU_1's probing actually acts as a full duplex relay.

In practice, it usually takes several time slots for PU transmitters to adjust their power to stable values p_1 and p_2. To facilitate our algorithm development, we assume that the transmission power of PUs can achieve stable values in one time slot.

B. Probing and Estimation

In this section, we will introduce the probing process in the time slots 1 and 3, then that in the time slots 2 and 4. Finally, we will obtain the estimations of h_1^2, h_2^2, and h_3^2.

1) Time Slots 1 and 3: In the time slot 1, PU_1 transmits a signal to PU_2, the received signal and the corresponding SNR at CU_1 can be expressed as

$$y_{r_1}(k) = \sqrt{p}h_3x(k) + n_r(k) \tag{6}$$

and

$$\gamma_{r1} = \frac{ph_3^2}{\sigma^2}, \tag{7}$$

where $n_r(k)$ represents the AWGN at CU_1.

Upon the received primary signal from PU_1, CU_1 amplifies and forwards the signal to PU_2 with the amplitude gain G_2. The probing signal can be expressed as

$$x_c(k) = G_2(\sqrt{p}h_3x(k) + n_r(k)). \tag{8}$$

Then the received signal at PU_2 becomes

$$y_2(k) = \underbrace{\sqrt{p}h_1x(k)}_{\text{Direct link signal}} + \underbrace{h_2G_2(\sqrt{p}h_3x(k) + n_r(k))}_{\text{Relay link signal}} + \underbrace{n_2(k)}_{\text{AWGN}} \tag{9}$$

and the SNR at PU_2 can be expressed as

$$\gamma_2 = \frac{p(h_1 + G_2h_2h_3)^2}{\sigma^2(G_2^2h_2^2 + 1)}. \tag{10}$$

Obviously, CU_1 can improve the SNR at PU_2 with a proper gain G_2, which will be selected in the next section through simulation.

In the time slot 2, PU_2 will send a control signal back to PU_1, based on which PU_1 determines the transmission power in the time slot 3 as

$$p_1 = \frac{\gamma_T\sigma^2(G_2^2h_2^2 + 1)}{(h_1 + G_2h_2h_3)^2}. \tag{11}$$

Then CU_1 obtains an updated SNR, i.e.,

$$\gamma_{r_1}^{'} = \frac{p_1h_3^2}{\sigma^2}. \tag{12}$$

2) Time Slots 2 and 4: Similarly, in the reverse transmission, if CU_1 amplifies the received primary signal with the gain G_1, CU_1 will obtain a SNR γ_{r_2} in the time slot 2 and an updated one $\gamma_{r_2}^{'}$ in the time slot 4, i.e.,

$$\gamma_{r_2} = \frac{ph_2^2}{\sigma^2} \tag{13}$$

and

$$\gamma_{r_2}^{'} = \frac{p_2h_2^2}{\sigma^2}, \tag{14}$$

where

$$p_2 = \frac{\gamma_T \sigma^2 (G_1^2 h_3^2 + 1)}{(h_1 + G_1 h_2 h_3)^2}. \quad (15)$$

3) Estimation: At the beginning without probing, the targeted SNR at PUs can be expressed as

$$\gamma_T = \frac{p h_1^2}{\sigma^2}. \quad (16)$$

Comparing (7) with (16), we obtain

$$h_1^2 = \frac{\gamma_T h_3^2}{\gamma_{r_1}}. \quad (17)$$

Comparing (7) with (13), we obtain

$$h_2^2 = \frac{\gamma_{r_2} h_3^2}{\gamma_{r_1}}. \quad (18)$$

These indicate that the channel gains h_1^2 and h_2^2 can be derived from h_3^2. In the following, we will derive the estimation of h_3^2.

From (13) and (14), the updated transmission power of PU_2 can be expressed as

$$p_2 = \frac{\gamma_{r_2}^{'} p}{\gamma_{r_2}}. \quad (19)$$

Substitute (16)-(19) into (15), we have

$$G_1^2 \gamma_{r_2}^{'} \frac{h_3^2}{\gamma_T} + \frac{2 G_1 \gamma_{r_2}^{'}}{\sqrt{\gamma_{r_2}}} \frac{h_3}{\sqrt{\gamma_T}} + \frac{\gamma_{r_2}^{'}}{\gamma_{r_2}} - G_1^2 h_3^2 - 1 = 0. \quad (20)$$

From (7) and (12), the updated transmission power of PU_1 can be expressed as

$$p_1 = \frac{\gamma_{r_1}^{'} p}{\gamma_{r_1}}. \quad (21)$$

Substitute (16)-(18) and (21) into (11), we have

$$G_2^2 \gamma_{r_1}^{'} \frac{h_3^2}{\gamma_T} + \frac{2 G_2 \gamma_{r_1}^{'}}{\sqrt{\gamma_{r_2}}} \frac{h_3}{\sqrt{\gamma_T}} + \frac{\gamma_{r_1}^{'}}{\gamma_{r_2}} - G_2^2 h_3^2 - \frac{\gamma_{r_1}}{\gamma_{r_2}} = 0. \quad (22)$$

By combining the two equations (20) and (22), we obtain the channel gain estimation of h_3 as follows,

$$\hat{h}_3^2 = \gamma_{r_2}^{'} \kappa^2 + \frac{2 {\gamma_{r_2}}'}{G_1 \sqrt{\gamma_{r_2}}} \kappa + \frac{\gamma_{r_2}^{'}}{G_1^2 \gamma_{r_2}} - \frac{1}{G_1^2}, \quad (23)$$

where

$$\kappa = \frac{\frac{\gamma_{r_2}^{'}}{G_1} - \frac{\gamma_{r_1}^{'}}{G_2} \pm \sqrt{\gamma_{r_1}^{'} \gamma_{r_2}^{'} (\frac{1}{G_2} - \frac{1}{G_1})^2 + (\gamma_{r_1}^{'} - \gamma_{r_2}^{'})(\frac{\gamma_{r_1}}{G_2^2} - \frac{\gamma_{r_2}}{G_1^2})}}{(\gamma_{r_1}^{'} - \gamma_{r_2}^{'}) \sqrt{\gamma_{r_2}}}. \quad (24)$$

From (24), the estimation may fail if both roots are negative or non-real due to SNR measurement errors, improper values of G_1 and G_2, etc. Then, we only consider the success estimations that are positive and real. In addition, we may also obtain two success estimations. If this happens, we will randomly pick one of them since it is quite complicated to select the roots and the random-pick method has already achieved reasonable performance.

Consequently, the channel gain estimations of h_2 and h_1 can be derived from (17), (18), and (23) as

$$\hat{h}_2^2 = \frac{\gamma_{r2}^{'}}{G_1^2 \gamma_{r1}} + \frac{\gamma_{r2}^{'} \gamma_{r2} \kappa^2}{\gamma_{r1}} + \frac{2 {\gamma_{r2}}' \kappa \sqrt{\gamma_{r2}}}{G_1 \gamma_{r1}} - \frac{\gamma_{r2}}{G_1^2 \gamma_{r1}}, \quad (25)$$

and

$$\hat{h}_1^2 = \frac{\left[\frac{\gamma_{r2}^{'}}{G_1^2 \gamma_{r2}} + \gamma_{r2}^{'} \kappa^2 + \frac{2 {\gamma_{r2}}' \kappa}{G_1 \sqrt{\gamma_{r2}}} - \frac{1}{G_1^2} \right]^2}{\kappa^2 \gamma_{r1}}, \quad (26)$$

respectively. In the next section, we will provide the simulation results to show the performance of the estimations.

C. Discussion

In this subsection, we will investigate the difference when CU_1 transmits probing signal using received primary signal or generated jamming signal.

When the jamming signal is used for probing, the overall received signal at PU_2 in (9) reduces to

$$y_2^{\mathrm{J}}(k) = \underbrace{\sqrt{p} h_1 x(k)}_{\text{Direct link signal}} + \underbrace{\sqrt{p_I} h_2 x_I(k)}_{\text{Jamming}} + \underbrace{n_2(k)}_{\text{AWGN}}, \quad (27)$$

where p_I denotes the power of the jamming probing signal $x_I(k)$. Accordingly, the received SINR at PU_2 in (10) becomes

$$\gamma'^{J} = \frac{p h_1^2}{\sigma^2 + p_I h_2^2}. \quad (28)$$

Under CLPC, PU_1 will adjust its transmission power to p_1^J to satisfy a targeted SINR,

$$\gamma_T = \frac{p_1^J h_1^2}{\sigma^2 + p_I h_2^2}. \quad (29)$$

Thus, the adjusted transmission power of PU_1 in (11) and the CU_1's updated SNR in (12) becomes

$$p_1^J = \frac{\gamma_T (\sigma^2 + p_I h_2^2)}{h_1^2} \quad (30)$$

and

$$\gamma_{r1}^{'} = \frac{p_1^J h_3^2}{\sigma^2}. \quad (31)$$

By comparing (16) and (29), we have

$$\frac{p}{p_1^J} = \frac{\sigma^2}{\sigma^2 + p_I h_2^2}, \quad (32)$$

which cancels h_1^2.

By comparing (7) and (31), we have

$$\frac{p}{p_1^J} = \frac{\gamma_{r1}}{\gamma_{r1}^{'}}, \quad (33)$$

which cancels h_3^2.

Based on (32) and (33), the estimation becomes

$$\frac{h_2^2}{\sigma^2} = \frac{\gamma_{r1}^{'} - \gamma_{r1}}{\gamma_{r1} p_I}, \quad (34)$$

which is the same as (15) in [2]. From (34), the estimation can only obtain the ratio between h_2^2 and the noise power at PU_2.

Similarly, if we consider the transmission from PU_2 to PU_1, we may obtain the estimation of h_3^2/σ^2. However, there is no way to obtain the estimation regarding h_1^2 if CU_1 does not use the received PU signal for probing. This is because h_1^2 is canceled in (32).

IV. Simulation Results

A. Assumptions

The system model in Section II is used in our simulation. In particular, the two PUs and CU_1 are considered to be in a line, where the distance between PU_1 and PU_2 is 0.25 km and the distance between PU_1 and CU_1 is denoted as d, 0.035 km $\leq d \leq$ 0.215 km. The transmitted signal suffers shadowing and path loss in wireless channels. The shadowing follows log-normal distribution with variance $\sigma_s^2 = 10$ and the path loss follows [9]

$$P_L(\text{dB}) = 128.1 + 37.6\log_{10}(l), \quad l \geq 0.035 \text{ km}, \qquad (35)$$

where l denotes the distance from a transmitter to a receiver. The targeted SNR of PUs is 10 dB, the bandwidth is 1 MHz, the noise power is -114 dBm, 100 samples are used to measure a SNR, and 10000 Monte Carlo trails are performed for each curve.

The relative estimation error is defined as

$$\epsilon = \frac{\left|10\log_{10}(\hat{h}_i^2) - 10\log_{10}(h_i^2)\right|}{10\log_{10}(h_i^2)}, \quad i = 1, 2, 3, \qquad (36)$$

where $\hat{h}_i^2$ denotes the estimation of h_i^2.

As indicated in (23) and (24), the estimation of h_3^2 may have negative or non real solutions due to SNR measurement errors or improper values of G_1 and G_2. Then, the estimation of h_3^2 is feasible only when (23) is positive and real. Let N_m be the number of overall estimations and N_s be the number of feasible estimations, then the probability of success estimation can be expressed as $\eta = N_s/N_m$.

B. Parameters Selection

Fig. 4 shows the estimation performance on h_1^2 for different CU_1 amplification gains G_1 and G_2, where CU_1 is located in the middle of PU_1 and PU_2, i.e., $d = 125$ m. From the figure, the good performance with small estimation error can be achieved when $G_1 = G_2$. For the other two channels, i.e., h_2^2 and h_3^2, the similar results can be achieved and they are omitted due to the limited pages of this paper.

Fig. 5 provides the detailed performance of Fig. 4 when $G_1 = G_2$. The estimation performance on h_2^2 and h_3^2, and the probability of success estimation are also provided. From the figure, the relative estimation error of h_1^2 is larger than that of h_2^2 and h_3^2, where the curves of h_2^2 and h_3^2 are overlapping. When $G_1 = G_2$ is smaller than about 50 dB, the relative estimation error decreases as G_1 or G_2 grows. When $G_1 = G_2$ is larger than about 50 dB, the relative estimation error increases as G_1 or G_2 grows. Thus, the optimal G_1 and G_2 for h_2^2 and h_3^2 equal to 47 dB and those for h_1^2 equals to 50 dB.

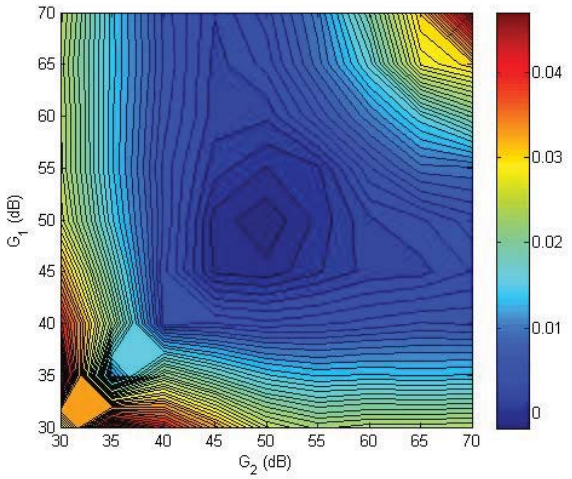

Fig. 4. Relative estimation error on h_1^2 versus different G_1 and G_2, where $d = 125$m.

Regarding the probability of success estimation, it achieves the best performance when $G_1 = G_2 = 47$ dB.

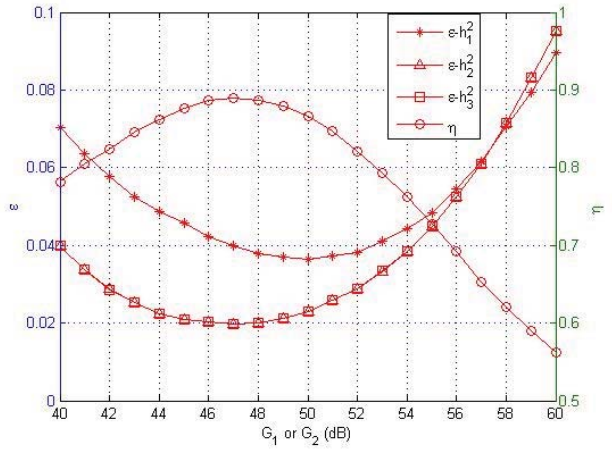

Fig. 5. Relative estimation errors on h_1^2, h_2^2, and h_3^2, where $G_1 = G_2$ and $d = 125$m.

Fig. 6 shows the optimal G_1 and G_2 for different locations of CU_1. When minimizing the estimation error of h_2^2 or h_3^2, G_1 always equals to G_2. As CU_1 moves from PU_1 to PU_2, G_1 and G_2 increase from 45 dB to 47 dB for $d \leq 0.08$ km, keep 47 dB for 0.08 km $\leq d \leq$ 0.17 km, and decrease from 47 dB to 45 dB for 0.17 km $\leq d \leq$ 0.215 km. When minimizing the estimation error of h_1^2, G_1 increases from 48 dB to 50 dB while G_2 increases from 45 dB to 50 dB for 0.035 km $\leq d \leq$ 0.125 km. For 0.125 km $\leq d \leq$ 0.215 km, G_1 decreases from 50 dB to 45 dB while G_2 decreases from 50 dB to 48 dB.

C. Estimation Performance

In this subsection, we will demonstrate the estimation performance for different CU_1 locations, where the optimal

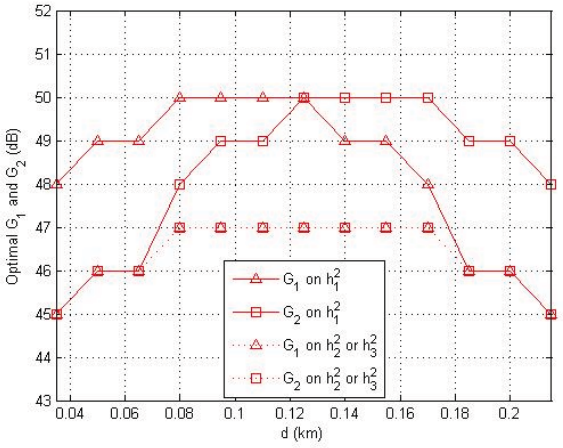

Fig. 6. Optimal G_1 and G_2 on h_1^2, h_2^2, and h_3^2.

G_1 and G_2 in Fig. 6 are applied to obtain the best estimation of h_1^2, h_2^2, and h_3^2. The probability of success estimation η is also provided.

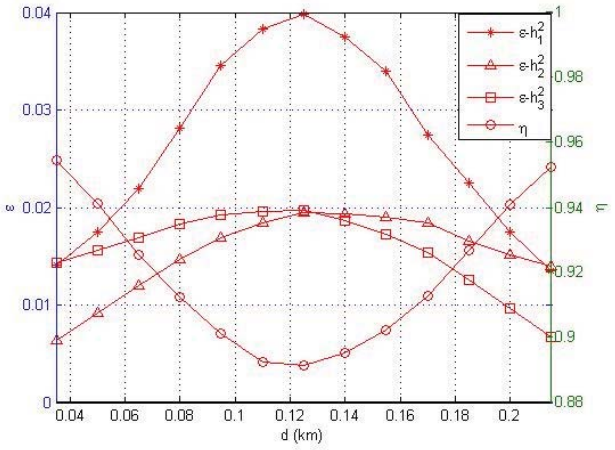

Fig. 7. Relative estimation errors of h_1^2, h_2^2, and h_3^2 for different CU_1 locations with optimal G_1 and G_2.

Fig. 7 illustrates the performance of the proposed approach versus different locations of CU_1. From the figure, the relative estimation error of h_1^2 is generally larger than that of h_2^2 and h_3^2. This is because h_2^2 and h_3^2 are estimated directly while h_1^2 is obtained based on h_2^2 or h_3^2, which introduces additional errors. Furthermore, all curves of the relative estimation error grow as the distance between CU_1 and PU_1 d increases from 0.035 km to 0.125 km, while the performance decreases as the distance d keeps on increasing from 0.125 km to 0.215 km. This is reasonable since when CU_1 is close to PU_1 or PU_2, it will enlarge the path loss difference of h_2^2 and h_3^2 as well as the PU_1's and PU_2's power adjustment due to CU_1 probing. As a result, the SNR difference in (24), i.e., $\gamma'_{r1} - \gamma'_{r2}$, will grow, which makes the estimation more robust to the SNR measurement errors. Thus, if CU_1 is close to PU_1 or PU_2, the relative estimation errors are below 0.02, where the range of channel gains is from about -120 dB to about -50 dB.

For the probability of success estimation, it is above 89%. Specifically, it achieves good performance when CU_1 is close to PU_1 or PU_2, and bad performance when CU_1 is in the middle of PU_1 and PU_2.

V. Conclusions

This paper has proposed a proactive channel gain estimation approach without information exchange between cognitive and primary users. By using the received primary signal for probing, a cognitive user can estimate not only the channel gain from a cognitive user to a primary receiver but also that between two primary users. In particular, the probing in the estimation is interference-free to primary users. Our study has also shown that using the received PU signal for probing is a requirement to estimate the channel gain between two primary users. With the proposed approach, cognitive users are able to realize the coexistence between primary and cognitive users.

References

[1] S. Haykin, "Cognitive radio: Brain-empowered wireless communications," *IEEE J. Select. Areas Commun*., vol. 23, no. 2, pp. 201-220, Feb. 2005.

[2] R. Zhang, "On active learning and supervised transmission of spectrum sharing based cognitive radios by exploiting hidden primary radio feedback," *IEEE Trans. Commun.*, vol. 58, no. 10, pp. 2960-2970, Oct. 2010.

[3] I. F. Akydiz, W.-Y. Lee, M. C. Vuran, and S. Mohanty, "Next generation/dynamic spectrum access/cognitive radio wireless networks: A survey," *IEEE Computer Networks*, vol. 50, Issue 13, pp. 2127-2159, May 2006.

[4] N. Devroye, P. Mitran, and V. Tarokh, "Achievable rates in cognitive channels," *IEEE Trans. Inf. Theory*, vol. 52, no. 5, pp. 1813-1827, May 2006.

[5] W. Wu, S. Vishwanath, and A. Arapostathis, "Capacity of a class of cognitive radio channels: Interference channels with degraded message sets," *IEEE Trans. Inf. Theory*, vol. 53, no. 11, pp. 4391-4399, Nov. 2007.

[6] J. Jiang and Y. Xin, "On the achievable rate regions for interference channels with degraded message sets," *IEEE Trans. Inf. Theory*, vol. 54, no. 10, pp. 4707-4712, Oct. 2008.

[7] G. Zhao, G. Li, and C. Yang, "Proactive detection of spectrum opportunities in primary systems with power control," *IEEE Trans. Wireless Commun.*, vol. 8, Issue. 9, pp. 4815-4823, Sept. 2009.

[8] I. Bajaj and Y. Gong, "Cross-channel estimation using supervised probing and sensing in cognitive radio networks," *in Proc. IEEE Int. Commun. Conf.* (ICC), Jun. 2011, pp. 1-5.

[9] 3GPP TR 25.814, Physical layer aspects for evolved univeral terrestrial radio access (UTRA), 2006.

Towards the Feasibility Conditions for Linear Interference Alignment with Symbol Extensions: A Diversity Constraint

Liangbin Li, Hamid Jafarkhani, Syed Ali Jafar

Center for Pervasive Communications & Computing, University of California, Irvine

***Abstract*—We explore the feasibility of linear interference alignment using finite signaling dimensions and symbol extensions. In the *non-zero total intersection* regime, we show that the number of sources is upperbounded by a function of *channel diversity*. The available diversity places a fundamental constraint on the number of signal spaces that can overlap at one destination (where they are undesired) while maintaining the resolvability of a subset of those signals (desired signals) at another destination. Specifically, the number of such signal spaces cannot be larger than the channel diversity. This is the *diversity constraint* that we identify in this paper. Not only is the proposed method applicable for X channels, interference channels, and their rank-deficient counterparts, it can also be used for both circular symmetric signaling (CSS) and asymmetric complex signaling (ACS) over a combination of frequency and MIMO channels with arbitrary symbol extensions.**

I. Introduction

Interference alignment is an effective technique to tackle the problem of interference in multi-user networks [1]–[4]. While interference seems to bound the growth of the degree of freedom (DoF) gain, in [1], Cadambe and Jafar surprisingly show that a total DoF gain of $\frac{K}{2}$ is asymptotically achievable for the K-user interference channels. The achievable scheme is based on *asymptotic alignment*, and it achieves the general outerbound on the DoF gain with a simple linear structure. Using this idea for the X channels where both the number of sources and the number of destinations are greater than two, the asymptotic alignment can also achieve the general outerbound [2]. The asymptotic alignment method requires infinite spectrum and *time-varying channels*, i.e., the channel value in each channel use is independently distributed, which is hard to justify in practice. This motivates the study of linear alignment using finite signaling dimensions.

In general, the feasibility of linear alignment using finite dimensions is still an open problem except in the case of single channel use and few other special cases. For the three-user interference channels, the feasibility using finite frequency dimensions is characterized in [5]. The achievable total DoF gain is shown to be a function of *channel diversity*, which represents the richness of independent channels in the signaling spectrum. For the general K-user MIMO interference channels with M transmit antennas and N receive antennas, feasibility is only discussed without symbol extensions. The total DoF gain is bounded by $\mathcal{D} \leq \frac{K(M+N)}{K+1}$ through comparing the number of variables and equations in [6]. The bound is proved to be necessary for linear interference alignment assuming no symbol extension and circular symmetric signaling (CSS) [7], [8]. This is in contrast to the results of the asymptotic alignment, where the total DoF gain grows linearly with K. However, since symbol extension is not used, it is not clear if the bound still holds for finite symbol extensions. As shown in [4], channel extension can improve the DoF gain of the constant three-user interference channels from 1 to $\frac{6}{5}$. It would be desirable to have a general method to check the feasibility for both X and interference channels using asymmetric complex signaling (ACS) [4] over a combination of frequency and MIMO channels with extensions. In this paper, we propose a method to fulfill this gap.

The rest of the paper is organized as follows. Section II discusses the use of channel dimensions and signaling methods. In Section III, we redefine channel diversity and show a theorem on the dimension of the subspace spanned by channel matrices. Section IV provides applications of the theorem to evaluate feasibility for different channel models. Conclusions are given in Section V.

Notations: We use capitalized letters $\mathbf{A} \in \mathbb{C}^{m\times n}$ and $\bar{\mathbf{A}} \in \mathbb{R}^{m\times n}$ (with a top bar) to denote a matrix drawn from the $m \times n$ matrix space defined on complex fields and a matrix in the $m \times n$ matrix space defined on real fields, respectively. We also use $\mathrm{Re}(x)$, $\mathrm{Im}(x)$, $\mathbf{E}_n$, $\otimes$, $\mathbf{A}^{\mathrm{T}}$, $\mathrm{span}(\mathbf{A})$, and $\mathrm{vec}(\mathbf{A})$ to denote real and imaginary components of $x \in \mathbb{C}$, an identity matrix of size $n \times n$, tensor product, transpose, column span, and vectorization of matrix $\mathbf{A}$, respectively. The notations $\bigcap$, $\setminus$, and $\mathbb{N}(z)$ are used for set intersection, set complement, and the set of natural number from 1 to z with $z \in \mathbb{N}^+$, respectively.

II. Channel Dimensions

Consider a wireless multi-user network with J sources and N destinations. All sources and destinations are equipped with M antennas, and the signals are transmitted over the

This work was supported in part by the NSF award CCF-0963925.

same F frequency tones. The channel matrix from Source j to Destination i at Frequency Tone f can be described by $\mathbf{H}^{jif} \in \mathbb{C}^{M\times M}$, where $j \in \mathbb{N}(J), i \in \mathbb{N}(N), f \in \mathbb{N}(F)$ are denoted as the indices for source, destination, and frequency, respectively. It follows that $M = 1$ corresponds to only using frequency channels and $F = 1$ corresponds to only using spatial channels. The (n, m)th entry of $\mathbf{H}^{jif}$, denoted as h^{jif}_{nm}, is the fading coefficient from transmit Antenna m to receive Antenna n. The distribution of h^{jif}_{nm} depends on the channel model, and will be described later. For convenience, we denote $\mathbf{H}^{ji} \in \mathbb{C}^{MF\times MF}$ to be the channel matrix from Source j to Destination i by aggregating channels of all frequency tones. The matrix $\mathbf{H}^{ji}$ has a block diagonal structure, i.e., $\mathbf{H}^{ji} = \text{diag}\,(\mathbf{H}^{ji1}, \mathbf{H}^{ji2}, \ldots, \mathbf{H}^{jiF})$. We assume that all channel matrices are known at all sources.

Let the symbol extension be T channel uses and the transmitted block from Source j be $\mathbf{X}^j \in \mathbb{C}^{MF\times T}$. Assume that all channel matrices $\mathbf{H}^{ji}$ keep unchanged during the transmission. The signal block at Destination i can be written as

$$\mathbf{Y}^i = \sum_{j\in\mathbb{N}(J)} \mathbf{H}^{ji}\mathbf{X}^j + \mathbf{W}^i,\ i \in \mathbb{N}(N), \tag{1}$$

where $\mathbf{Y}^i, \mathbf{W}^i \in \mathbb{C}^{MF\times T}$ denotes the receive signal block and additive white Gaussian noise (AWGN) matrix at Destination i, respectively. All the entries in $\mathbf{W}^i$ are i. i. d. $\mathcal{CN}(0, 1)$ distributed. The system equation in (1) can be converted to a vector form as

$$\underbrace{\text{vec}(\mathbf{Y}^i)}_{\mathbf{y}^i} = \sum_{j\in\mathbb{N}(J)} \underbrace{\mathbf{E}_T \otimes \mathbf{H}^{ji}}_{\mathcal{H}^{ji}} \underbrace{\text{vec}(\mathbf{X}^j)}_{\mathbf{x}^j} + \underbrace{\text{vec}(\mathbf{W}^i)}_{\mathbf{w}^i}, \tag{2}$$

where $\mathbf{y}^i, \mathbf{x}^j, \mathbf{w}^i \in \mathbb{C}^{MFT\times 1}$, and $\mathcal{H}^{ji} \in \mathbb{C}^{MFT\times MFT}$ is the equivalent channel matrix capturing spatial, frequency, and time dimensions. We call (2) the extended system equation for CSS, since complex symbols are linearly embedded into $\mathbf{x}^j$. By T symbol extensions, each source and destination has aggregated MFT signaling dimensions.

The idea of ACS has been used extensively in the space-time coding literature [9] and is proposed for interference alignment in [4]. The real and imaginary components of one complex symbol are independently embedded into $\mathbf{x}^j$. ACS falls into the class of linear alignment. In what follows, we will introduce an extended system equation for ACS. Let the tth entries of $\mathbf{y}^i, \mathbf{x}^j, \mathbf{w}^i$ be y^i_t, x^j_t, w^i_t, respectively, where $t \in \mathbb{N}(MFT)$. Denote

$$\bar{\mathbf{y}}^i = \left[\ \text{Re}(y^i_1)\ \ \text{Im}(y^i_1)\ \ \cdots\ \ \text{Re}(y^i_{MFT})\ \ \text{Im}(y^i_{MFT})\ \right]^{\text{T}}$$
$$\bar{\mathbf{x}}^j = \left[\ \text{Re}(x^j_1)\ \ \text{Im}(x^j_1)\ \ \cdots\ \ \text{Re}(x^j_{MFT})\ \ \text{Im}(x^j_{MFT})\ \right]^{\text{T}}$$
$$\bar{\mathbf{w}}^i = \left[\ \text{Re}(w^i_1)\ \ \text{Im}(w^i_1)\ \ \cdots\ \ \text{Re}(w^i_{MFT})\ \ \text{Im}(w^i_{MFT})\ \right]^{\text{T}},$$

where $\bar{\mathbf{y}}^i, \bar{\mathbf{x}}^j, \bar{\mathbf{w}}^i \in \mathbb{R}^{2MFT\times 1}$. The system equation in (2) can be rewritten as

$$\bar{\mathbf{y}}^i = \sum_{j\in\mathbb{N}(J)} \underbrace{\mathbf{E}_T \otimes \bar{\mathbf{H}}_{ji}}_{\bar{\mathcal{H}}^{ji}} \bar{\mathbf{x}}^j + \bar{\mathbf{w}}^i, \tag{3}$$

TABLE I
CHANNEL DIVERSITY d FOR DIFFERENT SIGNALING METHODS

Signaling methods	ACS	CSS
Channel diversity d	$2FM^2$	FM^2

where $\bar{\mathcal{H}}^{ji} \in \mathbb{R}^{2MFT\times 2MFT}, \bar{\mathbf{H}}^{ji} \in \mathbb{R}^{2MF\times 2MF}$ with

$$\bar{\mathbf{H}}^{ji} = \text{diag}\,(\bar{\mathbf{H}}^{ji1}, \bar{\mathbf{H}}^{ji2}, \ldots, \bar{\mathbf{H}}^{jiF}), \tag{4}$$
$$\bar{\mathbf{H}}^{jif} = \begin{bmatrix} \text{Re}(h^{jif}_{11}) & -\text{Im}(h^{jif}_{11}) & \cdots & \text{Re}(h^{jif}_{1M}) & -\text{Im}(h^{jif}_{1M}) \\ \text{Im}(h^{jif}_{11}) & \text{Re}(h^{jif}_{11}) & \cdots & \text{Im}(h^{jif}_{1M}) & \text{Re}(h^{jif}_{1M}) \\ \vdots & \vdots & \ddots & \vdots & \vdots \\ \text{Re}(h^{jif}_{M1}) & -\text{Im}(h^{jif}_{M1}) & \cdots & \text{Re}(h^{jif}_{MM}) & -\text{Im}(h^{jif}_{MM}) \\ \text{Im}(h^{jif}_{M1}) & \text{Re}(h^{jif}_{M1}) & \cdots & \text{Im}(h^{jif}_{MM}) & \text{Re}(h^{jif}_{MM}) \end{bmatrix}.$$

The 2×2 submatrices in $\bar{\mathbf{H}}^{jif}$ follow the real 2×2 orthogonal designs (real Alamouti structures) [9]. We call (3) the extended system equation for ACS. For CSS, the transmit and receive operations are in the MFT-dimensional vector space on complex fields; whereas for ACS, the operations are in the $2MFT$-dimensional vector space on real fields.

III. CHANNEL DIVERSITY

In this section, we extend the notion of channel diversity to incorporate the combination of frequency and MIMO channels. A theorem on the dimension of the subspace spanned by channel matrices is provided. Throughout the paper, we will only describe systems and prove theorems for the case of ACS. Extension to CSS is straightforward, since the important factor that affects the results is the diversity carried in the channel matrices, not the signaling method.

We assume that each entry in $\mathbf{H}^{jif}$ is independently drawn from a circular distribution, where the real and imaginary components of random variables are i. i. d.. The matrix $\mathbf{H}^{jif}$ is also independently drawn across frequency. Regarding channel matrices from different sources to destinations, we assume that they are linearly independent in the matrix space $\mathbb{C}^{M\times M}$. In other words, $\mathbf{H}^{jif} \neq \lambda\mathbf{H}^{luf}$ for $(j, i) \neq (l, u)$ and $\lambda \in \mathbb{C}$. We need to emphasize that $\mathbf{H}^{jif}$ may be correlated for different sources or destinations, as will be clarified later.

The notion of channel diversity is introduced in [5] for frequency channels to describe the richness of independent channels in the signaling spectrum. We generalize the notion to include both frequency and MIMO channels.

Definition 1: Channel diversity d is defined as the number of independent complex variables in $\mathbf{H}^{ji}$ for CSS and the number of independent real variables in $\bar{\mathbf{H}}^{ji}$ for ACS.

Table. I compares channel diversities for two signaling methods. ACS provides twice channel diversity compared to CCS. For example, when only frequency channels and ACS are used, i.e. $M = 1$, the channel matrix $\bar{\mathbf{H}}^{ji}$ in (4) becomes block diagonal with 2×2 submatrices on the diagonals. For the fth submatrix, it has only two independent variables $\text{Re}(h^{jif}_{11})$ and $\text{Im}(h^{jif}_{11})$. Since there are F submatrices on the diagonals, in total, the number of independent variables are $2F$.

With this definition, we are ready to present a theorem.

***Theorem** 1:* The subspace spanned by all $\bar{\mathbf{H}}^{ji}, j \in \mathbb{N}(J), i \in \mathbb{N}(N)$ has a dimension of at most d in the $\mathbb{R}^{2MF\times 2MF}$ matrix space.

Proof: It suffices to show that any $\bar{\mathbf{H}}^{ji}$ for $j > d$ can be written as linear combination of $\bar{\mathbf{H}}^{ji}$ for $j \in \mathbb{N}(d)$. In other words, there exists $c_l \in \mathbb{R}$ such that

$$\sum_{l\in\mathbb{N}(d)} c_l \bar{\mathbf{H}}^{li} = \bar{\mathbf{H}}^{ji}, j > d. \tag{5}$$

Let $\bar{\mathbf{H}}_{\mathrm{o}}^{jif} \in \mathbb{R}^{2M\times M}$ denote a matrix having the odd columns of $\bar{\mathbf{H}}^{jif}$ and $\tilde{\mathbf{H}}_{\mathrm{o}}^{ji} = \mathrm{vec}\left[\bar{\mathbf{H}}_{\mathrm{o}}^{ji1}, \bar{\mathbf{H}}_{\mathrm{o}}^{ji2}, \cdots, \bar{\mathbf{H}}_{\mathrm{o}}^{jiF}\right]$, where $\tilde{\mathbf{H}}_{\mathrm{o}}^{ji} \in \mathbb{R}^{2M^2F\times 1}$. Since the even columns of $\bar{\mathbf{H}}^{jif}$ are the permutations of the odd columns, they can be discarded in the process of finding the coefficients c_l. Eqn. (5) can be rewritten as

$$\sum_{l\in\mathbb{N}(d)} c_l \tilde{\mathbf{H}}_{\mathrm{o}}^{li} = \tilde{\mathbf{H}}_{\mathrm{o}}^{ji}. \tag{6}$$

The above vector equation consists of $2M^2F = d$ linearly independent scalar equations and d unknown variables c_l. Since fading coefficients are independently drawn across frequency and linear independent for different sources, the matrix $\left[\tilde{\mathbf{H}}_{\mathrm{o}}^{1i}, \tilde{\mathbf{H}}_{\mathrm{o}}^{2i}, \cdots, \tilde{\mathbf{H}}_{\mathrm{o}}^{di}\right]$ is almost surely full rank. It follows that the linear equations are solvable to find c_l. This concludes the proof. ∎

Remark: For CSS, the subspace spanned by all $\mathbf{H}^{ji}, j \in \mathbb{N}(J), i \in \mathbb{N}(N)$ has a dimension of at most d in the $\mathbb{C}^{MF\times MF}$ matrix space.

The theorem says that the number of resolvable channel matrices is limited by the channel diversity. If the number of channel matrices is higher than the channel diversity, channel matrices are linearly dependent in the matrix space and cannot be decoupled. For interference alignment, each destination needs to decouple its desired symbols, which translates to the resolvability of the signal subspace from the interference subspace. This motivates the use of Theorem 1 for the feasibility conditions of linear interference alignment.

IV. Applications to Feasibility

In this section, we show how Theorem 1 can be used to evaluate the feasibility conditions of X channels, interference channels, and their rank-deficient counterparts. We will describe the application for X channels in details, and simplify the writing for other channels. Subsections IV-A, IV-B, and IV-C provide feasibility conditions for X channels, interference channels, and rank-deficient counterparts, respectively.

A. X channels

We consider a symmetric scenario where each source sends a DoF gain of $D \in \mathbb{R}$ to each destination per dimension, i.e., per tone, per antenna, and per channel use. Note that one real symbol carries $\frac{1}{2}$ DoF gain. Over F frequency tones, M antennas, and T symbol extensions, each source sends $\bar{D} = \lceil 2D \rceil MFT$ real symbols to each of the N destinations. In total, $\bar{D}N$ symbols are transmitted from each source.

1) Linear alignments: Let the kth real symbol intended for Destination i from Source j be s_k^{ji} where $k \in \mathbb{N}(\bar{D})$. Symbols are transmitted using linear beamforming

$$\bar{\mathbf{x}}^j = \sum_{i\in\mathbb{N}(N), k\in\mathbb{N}(\bar{D})} \bar{\mathbf{v}}_k^{ji} s_k^{ji}, \tag{7}$$

where $\bar{\mathbf{v}}_k^{ji} \in \mathbb{R}^{2MFT\times 1}$ denotes the transmit beamforming vectors for symbol s_k^{ji}. Then, the equivalent system equation in (3) can be rewritten by inserting (7)

$$\bar{\mathbf{y}}^i = \sum_{j,k} \bar{\mathcal{H}}^{ji} \bar{\mathbf{v}}_k^{ji} s_k^{ji} + \sum_{j,k,u\neq i} \bar{\mathcal{H}}^{ji} \bar{\mathbf{v}}_k^{ju} s_k^{ju} + \bar{\mathbf{w}}^i, \tag{8}$$

where the first term corresponds to desired symbols and the second term corresponds to interference. The total dimensions observed by each destination is $2MFT$. Each destination needs to decode $\bar{D}J$ symbols, and is interfered by $\bar{D}J(N-1)$ symbols. The key idea of interference alignment is to compress the dimension of the interference subspace by projecting interference into an overlapping subspace, while maintaining the desired symbols resolvable from the interference. Specifically, to align interference and separate desired symbols, we need

(1) *Alignment Condition:* $\bar{D}J(N-1)$ interfering symbols are aligned into interference subspace,

(2) *Separability Condition:* At each destination, the desired $\bar{D}J$ symbols can be decoupled from each other and from the interference.

2) Non-zero total intersection regime: In this paper, we are interested in the non-zero total intersection regime, where interference from all sources overlaps in some subspace. Intuitively, when more interference overlaps, the dimension of the interference subspace is reduced, which provides more dimensions for the desired signals. Consequently, the total DoF gains can be improved. We provide the formal definition of the non-zero total intersection regime as follows

***Definition** 2:* We define the *non-zero total intersection* regime of the linear alignment methods in X channels as $D > \frac{J-1}{J(N+J-2)}$.

Let $\bar{\mathbf{V}}^{ji} = \left[\bar{\mathbf{v}}_1^{ji}, \bar{\mathbf{v}}_1^{ji}, \cdots, \bar{\mathbf{v}}_{\bar{D}}^{ji}\right]$ and $\bar{\mathbf{I}}^{ji} = \bar{\mathcal{H}}^{ji}\left[\bar{\mathbf{V}}^{j1}, \cdots, \bar{\mathbf{V}}^{j(i-1)}, \bar{\mathbf{V}}^{j(i+1)}, \cdots, \bar{\mathbf{V}}^{jN}\right]$, where $\bar{\mathbf{I}}^{ji} \in \mathbb{R}^{2MFT\times(N-1)\bar{D}}$. The column span of $\bar{\mathbf{I}}^{ji}$ is the interference subspace created by Source j at Destination i.

***Proposition** 1:* In the non-zero total intersection regime, interference subspace $\bar{\mathbf{I}}^{ji}$ from all sources overlaps at each destination. In other words, $\bigcap_{j\in\mathbb{N}(J)} \mathrm{span}(\bar{\mathbf{I}}^{ji}) \neq \emptyset$ for $i \in \mathbb{N}(N)$.

Proof: We prove by contradiction. Note that all $\bar{D}N$ beamforming vectors transmitted from the same source cannot be linearly dependent. Then, the dimension of interference subspace $\bar{\mathbf{I}}^{ji}$ is $\bar{D}(N-1)$. Assume that the intersection of the

interference subspaces $\bar{\mathbf{I}}^{ji}$ is a null space. Then, the total interference subspace, which is $\bigcup_{j\in\mathbb{N}(J)} \text{span}(\bar{\mathbf{I}}^{ji})$, has dimensions $I^i \geq \frac{J\bar{D}(N-1)}{J-1}$. The minimum dimension occurs when each interfering beamforming vector is aligned with beamforming vectors from $J-2$ other sources. Since each destination perceives a $2MFT$-dimensional signal space, it follows that the remaining dimension for the desired symbols, which is $J\bar{D}$, is upperbounded by $J\bar{D} \leq 2MFT - \frac{J\bar{D}(N-1)}{J-1}$. After some manipulations, it results in $D \leq \frac{\bar{D}}{2MFT} \leq \frac{J-1}{J(N+J-2)}$, which is contradictory to the assumption of the non-zero total intersection regime. ■

We need to emphasize that we can also define the non-zero partial intersection regime when interference from a certain number (not all) of sources overlaps. Feasibility can be evaluated based on the number of overlapped sources at each destination instead of J. Extension from the non-zero total intersection regime to the non-zero partial intersection regime is straightforward.

We are ready to show the following theorem.

***Theorem** 2:* When the linear alignment is applied to the non-zero total intersection regime of $J \times N$ X channels, both the number of sources and the number of destinations cannot be larger than the channel diversity, i.e., $\max\{J, N\} \leq d$.

Proof: The proof is also illustrated in Fig. 1. Let us focus on Destination i. Since the system operates in the non-zero total intersection regime, we describe the intersection of interference subspaces from different sources using a matrix $\bar{\mathbf{I}}^i_\cap$, where $\bar{\mathbf{I}}^i_\cap \in \mathbb{R}^{2MFT\times I^i_\cap}$ and its columns are the basis for the subspace. Then, we have $\text{span}(\bar{\mathbf{I}}^i_\cap) = \bigcap_{j\in\mathbb{N}(J)} \text{span}(\bar{\mathbf{I}}^{ji})$. From the alignment condition, at Source $j \in \mathbb{N}(J)$, there exist $I^i_\cap$ transmit beamforming vectors $\bar{\mathbf{v}}^{ju_j}_k, u_j \neq i$, such that $\bar{\mathcal{H}}^{ji}\bar{\mathbf{v}}^{ju_j}_k \in \text{span}(\bar{\mathbf{I}}^i_\cap)$. It follows that $\bar{\mathbf{v}}^{ju_j}_k \in \text{span}((\bar{\mathcal{H}}^{ji})^{-1}\bar{\mathbf{I}}^i_\cap)$, since the nonzero entries in $\bar{\mathcal{H}}^{ji}$ are independently drawn and hence $\bar{\mathcal{H}}^{ji}$ is invertible. Denote the set of the indices of these beamformers at Source j as S^{ji}, where $|S^{ji}| = I^i_\cap$. Now, let us look at Destination u_j, where $\bar{\mathbf{v}}^{ju_j}_k$ are the desired transmit beamformers. We use index l for sources other than j. The signal subspace created by $\bar{\mathbf{v}}^{ju_j}_k, k \in S^{ji}$ can be described by $\bar{\mathcal{H}}^{ju_j}(\bar{\mathcal{H}}^{ji})^{-1}\bar{\mathbf{I}}^i_\cap$, while the subspace created by other sources can be similarly described by $\bar{\mathcal{H}}^{lu_j}(\bar{\mathcal{H}}^{li})^{-1}\bar{\mathbf{I}}^i_\cap, l \neq j$. In what follows, we show $\bar{\mathbf{v}}^{ju_j}_k$ cannot be decoupled from the subspace $\bigcup_{l\neq j} \text{span}(\bar{\mathcal{H}}^{lu_j}(\bar{\mathcal{H}}^{li})^{-1}\bar{\mathbf{I}}^i_\cap)$ at Destination u_j if $J > d$. Then, the desired symbols cannot be extracted using zero-forcing, which violates the separability condition. It suffices to show that there exists coefficients $c_l \in \mathbb{R}$ such that

$$\sum_{l\in\mathbb{N}(d)} c_l\bar{\mathcal{H}}^{lu_j}(\bar{\mathcal{H}}^{li})^{-1}\bar{\mathbf{I}}^i_\cap = \bar{\mathcal{H}}^{ju_j}(\bar{\mathcal{H}}^{ji})^{-1}\bar{\mathbf{I}}^i_\cap,\ j > d. \tag{9}$$

Note that $\bar{\mathbf{H}}^{lu_j}(\bar{\mathbf{H}}^{li})^{-1}$ preserves the block diagonal structure of $\bar{\mathbf{H}}^{lu_j}$ and channel diversity. Then, from Theorem 1, there exists coefficients c_l for

$$\sum_{l\in\mathbb{N}(d)} c_l\bar{\mathbf{H}}^{lu_j}(\bar{\mathbf{H}}^{li})^{-1} = \bar{\mathbf{H}}^{ju_j}(\bar{\mathbf{H}}^{ji})^{-1},\ j > d. \tag{10}$$

By calculating the tensor product of both sides of the above equation with $\mathbf{E}_T$ and multiplying $\bar{\mathbf{I}}^i_\cap$ to both sides from the right, we result in (9). Therefore, we need $J \leq d$. Since linear alignments in X channels satisfy reciprocity [10] by reversing the communication direction, we also need $N \leq d$. This concludes the proof. ■

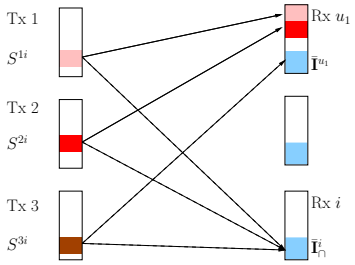

Fig. 1. Proof of Theorem 2 for 3×3 X channels. At destinations, light blue area denotes interference subspace. The solid line represents desired channels, while dashed line represents interfering channel. The desired signal (represented by pink block) need to be separable from other signals (represented by red and brown blocks).

***Corollary** 1:* For the constant single-antenna $J\times 2$ X channels with any symbol extensions, i.e., $M = 1, F = 1$, ACS is feasible in the non-zero total intersection regime for $J = 2$, while CSS is infeasible. Neither scheme is feasible for $J \geq 3$.

Proof: It is a straightforward application of Theorem 2 when $M = 1$ and $F = 1$. For ACS, the channel diversity is equal to 2. For CSS, the channel diversity is equal to 1. ■

The first statement in Corollary 1 is also claimed in [4] with the proof of achievability for ACS. Here, we also add the understandings of the limitation of ACS.

***Corollary** 2:* For the single-antenna $J\times 2$ X channels with 2 frequency tones and any symbol extensions, i.e., $M = 1, F = 2$, ACS is feasible only if $J \leq 4$, whereas CSS is feasible only if $J \leq 2$.

***Corollary** 3:* For the constant MIMO $J\times 2$ X channels with two antennas at each node and any symbol extensions, i.e., $M = 2, F = 1$, ACS is feasible only if $J \leq 8$, whereas CSS is feasible only if $J \leq 4$.

A comparison between Corollaries 2 and 3 implies that MIMO channels provide higher capability to accommodate users compared to frequency channels.

B. Interference channels

In K-user interference channels, each source sends symbols only to one distinct destination. We only need to remove the summation of i in (7), and linear transmission, e.g., alignment and separability conditions, are very similar to those of X channels. Since our system allows arbitrary symbol extensions

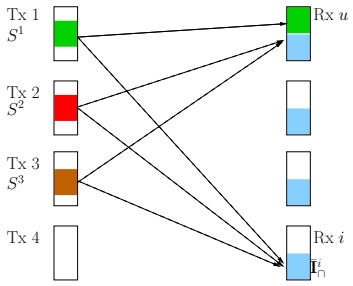

Fig. 2. Proof of Theorem 3 for 4-user interference channels. The desired signal (represented by green block) needs to be separable from interference (created by signals represented by red and brown blocks).

and ACS, it is different from [7], [8]. We adopt the same notations as in X channels. For interference channels, the desired symbols also need to be decoupled from the interference. Thus, we also need Theorem 1 to provide bounds on the dimension of the resolvable subspaces. The non-zero total intersection regime is defined first.

***Definition** 3:* We define the *non-zero total intersection* regime of the linear alignment methods in interference channels as $D > \frac{K-2}{2K-3}$.

In this rate regime, all interfering sources create overlapping subspaces at the undesired destinations. The proof is similar to that of Proposition 1, and is removed due to page limit.

***Theorem** 3:* When the linear alignment is applied to the non-zero total intersection regime of K-user interference channels, the number of users is bounded by $K \leq d+1$.

Proof: The proof is also illustrated in Fig. 2. Let us consider Destination i. Denote the intersection of the interference subspaces created by all sources as $\bar{\mathbf{I}}^i_\cap$, i.e., $\text{span}(\bar{\mathbf{I}}^i_\cap) = \bigcap_{j\in\mathbb{N}(K)\setminus\{i\}} \text{span}(\mathcal{H}^{ji}\bar{\mathbf{V}}^{jj})$. Then, at Source $j \in \mathbb{N}(K)\setminus\{i\}$, there exist some transmit beamformers which creates interference in $\bar{\mathbf{I}}^i_\cap$. Denote the set of indices k of such beamformers as S^j, i.e., $S^j = \{k|\bar{\mathbf{v}}^{jj}_k \in \text{span}((\mathcal{H}^{ji})^{-1}\bar{\mathbf{I}}^i_\cap), j \in \mathbb{N}(K)\setminus\{i\}\}$. Now, consider Destination u for the subspace created by beamformers in S^j from these sources. The subspace created by Source u is $\text{span}(\mathcal{H}^{uu}(\mathcal{H}^{ui})^{-1}\bar{\mathbf{I}}^i_\cap)$, which is for desired symbols. The subspace created by other interfering sources in $j \in \mathbb{N}(K)\setminus\{i,u\}$ is $\bigcup_j \text{span}(\mathcal{H}^{ju}(\mathcal{H}^{ji})^{-1}\bar{\mathbf{I}}^i_\cap)$. From the separability condition, the subspace of desired symbols needs to be linearly independent from the interference subspace. Note that there are $K-2$ interfering sources in $j \in \mathbb{N}(K)\setminus\{i,u\}$. From Theorem 1, the separability condition is violated if the number of interfering sources $K-2$ is no smaller than d. In other words, $K \leq d+1$. ■

C. Rank-deficient channels

In this subsection, we add another assumption on the correlation among channels from different sources to destinations. We assume that the channel matrix $\mathbf{H}^{jif}$ can be decomposed as $\mathbf{H}^{jif} = \mathbf{B}^{if}\mathbf{G}^{jf}$, where $\mathbf{B}^{if} \in \mathbb{C}^{M\times M_\text{R}}$, $\mathbf{G}^{jf} \in \mathbb{C}^{M_\text{R}\times M}$, and $M < M_\text{R} < \min(J,N)M$. All entries in $\mathbf{B}^{if}$ and $\mathbf{G}^{jf}$ are independently drawn from a circular distribution. The aggregation of channels from all nodes can be expanded as

$$\begin{bmatrix} \mathbf{H}^{11f} & \mathbf{H}^{21f} & \cdots & \mathbf{H}^{J1f} \\ \vdots & \vdots & \ddots & \vdots \\ \mathbf{H}^{1Nf} & \mathbf{H}^{2Nf} & \cdots & \mathbf{H}^{JNf} \end{bmatrix} = \begin{bmatrix} \mathbf{B}^{1f} \\ \vdots \\ \mathbf{B}^{Nf} \end{bmatrix} \begin{bmatrix} \mathbf{G}^{1f} & \cdots & \mathbf{G}^{Jf} \end{bmatrix}.$$

The aggregated channel matrix has rank M_R, hence is rank-deficient. This channel model can describe a two-hop relay channel where a full-duplex relay with M_R antennas performs amplify-and-forward. The matrices $\mathbf{G}^{jf}$ and $\mathbf{B}^{if}$ denote the source-relay channels and the relay-destination channels, respectively. The channel diversity for $\mathbf{G}^{jf}$ and $\mathbf{B}^{if}$ are equal to $d_\text{R} = 2MM_\text{R}F$ for ACS and $d_\text{R} = MM_\text{R}F$ for CSS.

***Theorem** 4:* When the linear alignment is applied to the non-zero total intersection regime of the $J \times N$ rank-deficient X channels, alignment is feasible only if $\max\{J,N\} \leq \min\{d, d_\text{R}-d+1\}$.

Proof: We only show $J \leq \min\{d, d_\text{R}-d+1\}$. The inequality $N \leq \min\{d, d_\text{R}-d+1\}$ follows from the communication reciprocity [10]. From the proof of Theorem 2, the number of sources is essentially bounded by the dimension of the subspace spanned by $\bar{\mathbf{H}}^{lu}(\bar{\mathbf{H}}^{li})^{-1}$ in the $\mathbb{R}^{2MF\times 2MF}$ matrix space for $l \in \mathbb{N}(J)$. A trivial outerbound on J is d, since $\bar{\mathbf{H}}^{lu}(\bar{\mathbf{H}}^{li})^{-1}$ is linearly independent in the matrix space for different values of l. In what follows, we explore the structure of $\mathbf{H}^{jif}$ and provide another bound $J \leq d_\text{R}-d+1$. Denote $d' = d_\text{R}-d+1$. We need to show that there exists $c_l \in \mathbb{R}$ such that

$$\sum_{l\in\mathbb{N}(d')} c_l\bar{\mathbf{H}}^{lu}(\bar{\mathbf{H}}^{li})^{-1} = \bar{\mathbf{H}}^{ju}(\bar{\mathbf{H}}^{ji})^{-1}, j > d'. \quad (11)$$

We need to establish some notations to prove this fact. Let $\mathbf{B}^{if} = \left[\mathbf{B}^{if}_1, \mathbf{B}^{if}_2\right]$ and $\mathbf{G}^{jf} = \left[(\mathbf{G}^{jf}_1)^\text{T}, (\mathbf{G}^{jf}_2)^\text{T}\right]^\text{T}$, where $\mathbf{B}^{if}_1, \mathbf{G}^{jf}_1 \in \mathbb{C}^{M\times M}$ and $\mathbf{B}^{if}_2, (\mathbf{G}^{jf}_2)^\text{T} \in \mathbb{C}^{M\times(M_\text{R}-M)}$. Separate the real and imaginary components and aggregate channels on different frequencies. Similar to $\bar{\mathbf{H}}^{ji}$ in (4), we can define $\bar{\mathbf{B}}^i_1, \bar{\mathbf{G}}^j_1 \in \mathbb{R}^{2MF\times 2MF}$ and $\bar{\mathbf{B}}^i_2, (\bar{\mathbf{G}}^j_2)^\text{T} \in \mathbb{R}^{2MF\times 2(M_\text{R}-M)F}$ as aggregations of $\mathbf{B}^{if}_1, \mathbf{G}^{jf}_1, \mathbf{B}^{if}_2$, and $\mathbf{G}^{jf}_2$, respectively. We can calculate

$$\begin{aligned}\bar{\mathbf{H}}^{lu}(\bar{\mathbf{H}}^{li})^{-1} &= \left(\left[\bar{\mathbf{B}}^u_1\ \bar{\mathbf{B}}^u_2\right]\begin{bmatrix}\bar{\mathbf{G}}^l_1 \\ \bar{\mathbf{G}}^l_2\end{bmatrix}\right)\left(\left[\bar{\mathbf{B}}^i_1\ \bar{\mathbf{B}}^i_2\right]\begin{bmatrix}\bar{\mathbf{G}}^l_1 \\ \bar{\mathbf{G}}^l_2\end{bmatrix}\right)^{-1} \\ &= \left[\bar{\mathbf{B}}^u_1\ \bar{\mathbf{B}}^u_2\right]\left(\begin{bmatrix}\mathbf{E} \\ \hat{\mathbf{G}}^l\end{bmatrix}\left(\mathbf{E}+\hat{\mathbf{B}}^i\hat{\mathbf{G}}^l\right)^{-1}\right)(\bar{\mathbf{B}}^i_1)^{-1},\end{aligned}$$

where $\hat{\mathbf{B}}^i = (\bar{\mathbf{B}}^i_1)^{-1}\bar{\mathbf{B}}^i_2$, $\hat{\mathbf{B}}^i \in \mathbb{R}^{2MF\times 2(M_\text{R}-M)F}$, and $\hat{\mathbf{G}}^l = \bar{\mathbf{G}}^l_2(\bar{\mathbf{G}}^l_1)^{-1}$, $\hat{\mathbf{G}}^l \in \mathbb{R}^{2(M_\text{R}-M)F\times 2MF}$. Since $\bar{\mathbf{B}}^u_1$, $\bar{\mathbf{B}}^u_2$, and $\bar{\mathbf{B}}^i_1$ are common to $\bar{\mathbf{H}}^{lu}(\bar{\mathbf{H}}^{li})^{-1}$ for different values of l, to show that (11) holds for some c_l, it suffices to find c_l for

$$\sum_{l\in\mathbb{N}(d')} c_l\begin{bmatrix}\mathbf{E} \\ \hat{\mathbf{G}}^l\end{bmatrix}\left(\mathbf{E}+\hat{\mathbf{B}}^i\hat{\mathbf{G}}^l\right)^{-1} = \begin{bmatrix}\mathbf{E} \\ \hat{\mathbf{G}}^j\end{bmatrix}\left(\mathbf{E}+\hat{\mathbf{B}}^i\hat{\mathbf{G}}^j\right)^{-1}. \quad (12)$$

When $M_{\mathrm{R}} \leq 2M$, the number of rows in $\hat{\mathbf{B}}^i$ is more than the number of its columns. Again, to show that (12) holds, it is sufficient to find c_l for

$$\sum_{l\in\mathbb{N}(d')} c_l \begin{bmatrix} \mathbf{E} \\ \hat{\mathbf{B}}^i\hat{\mathbf{G}}^l \end{bmatrix} \left(\mathbf{E}+\hat{\mathbf{B}}^i\hat{\mathbf{G}}^l\right)^{-1} = \begin{bmatrix} \mathbf{E} \\ \hat{\mathbf{B}}^i\hat{\mathbf{G}}^j \end{bmatrix} \left(\mathbf{E}+\hat{\mathbf{B}}^i\hat{\mathbf{G}}^j\right)^{-1}. \tag{13}$$

Note that $\hat{\mathbf{B}}^i\hat{\mathbf{G}}^l \left(\mathbf{E}+\hat{\mathbf{B}}^i\hat{\mathbf{G}}^l\right)^{-1} = \mathbf{E} - \left(\mathbf{E}+\hat{\mathbf{B}}^i\hat{\mathbf{G}}^l\right)^{-1}$. The above equation can be equivalently rewritten as

$$\sum_{l\in\mathbb{N}(d')} c_l \begin{bmatrix} \left(\mathbf{E}+\hat{\mathbf{B}}^i\hat{\mathbf{G}}^l\right)^{-1} \\ \mathbf{E} - \left(\mathbf{E}+\hat{\mathbf{B}}^i\hat{\mathbf{G}}^l\right)^{-1} \end{bmatrix} = \begin{bmatrix} \left(\mathbf{E}+\hat{\mathbf{B}}^i\hat{\mathbf{G}}^j\right)^{-1} \\ \mathbf{E} - \left(\mathbf{E}+\hat{\mathbf{B}}^i\hat{\mathbf{G}}^j\right)^{-1} \end{bmatrix},$$

which is identical to

$$\sum_{l\in\mathbb{N}(d')} c_l \left(\mathbf{E}+\hat{\mathbf{G}}^l\hat{\mathbf{B}}^i\right)^{-1} \hat{\mathbf{G}}^l = \left(\mathbf{E}+\hat{\mathbf{G}}^j\hat{\mathbf{B}}^i\right)^{-1} \hat{\mathbf{G}}^j \tag{14}$$

$$\sum_{l\in\mathbb{N}(d')} c_l = 1. \tag{15}$$

Since the size of $\left(\mathbf{E}+\hat{\mathbf{G}}^j\hat{\mathbf{B}}^i\right)^{-1}\hat{\mathbf{G}}^j$ is $2(M_{\mathrm{R}}-M)\times 2M$ and its 2×2 submatrices have real Alamouti structures, as we argue in the proof of Theorem 1, the number of linear independent scalar equations in (14) is $2(M_{\mathrm{R}}-M)M = d_{\mathrm{R}}-d$. Including (15), the total number is $d_{\mathrm{R}}-d+1$. Having $d' = d_{\mathrm{R}}-d+1$ unknown variables c_l can find a solution for c_l.

When $M_{\mathrm{R}} > 2M$, by a similar argument, we need at least $d_{\mathrm{R}}-d+1$ unknown variables to find a solution for c_l, because there are more equations to be satisfied in addition to (13). This concludes the proof. ■

***Theorem** 5:* When the linear alignment is applied to the non-zero total intersection regime of K-user rank-deficient interference channels, alignment is feasible only if $K \leq \min\{d+1, d_{\mathrm{R}}-d+2\}$.

Proof: The proof can be straightforwardly obtained by combining the proofs of Theorems 3 and 4. ■

V. Conclusion

This paper provides negative results for linear interference alignment using finite signaling dimensions and symbol extensions. We generalized the notion of channel diversity to incorporate both frequency and MIMO channels. Intuitively, channel diversity generates a limit on the number of signal subspaces that can overlap at one destination, while maintaining resolvability at another destination. Consequently, when sources are aligned at an interferring destination, they cannot be decoupled at a desired destination if the number of participating sources is greater than the available diversity. This reasoning leads to the proposed bounds in the non-zero total intersection regime: for $J \times N$ X channels, linear interference alignment is infeasible when $\max\{J,N\} > d$; for K-user interference channels, it is infeasible when $K > d+1$. Discussions on rank-deficient channels are also provided. We do not claim the achievability of the proposed outerbounds.

References

[1] V. Cadambe and S. Jafar, "Interference alignment and the degrees of freedom for the K user interference channel," *IEEE Transactions on Information Theory*, vol. 54, pp. 3425–3441, Aug. 2008.

[2] ——, "Interference alignment and the degrees of freedom of wireless X networks," *IEEE Transactions on Information Theory*, vol. 55, no. 9, pp. 3893 –3908, Sep. 2009.

[3] S. Jafar and S. Shamai, "Degrees of freedom region for the MIMO X channel," *IEEE Transactions on Information Theory*, vol. 54, no. 1, pp. 151–170, Jan. 2008.

[4] V. Cadambe, S. Jafar, and C. Wang, "Interference alignment with asymmetric complex signaling–settling the Host-Madsen-Nosratinia conjecture," *IEEE Transactions on Information Theory*, vol. 56, no. 9, pp. 4552 –4565, Sep 2010.

[5] G. Bresler and D. Tse, "3 user interference channel: Degrees of freedom as a function of channel diversity," in *47th Annual Allerton Conference on Communication, Control, and Computing, 2009.*, Oct. 2009, pp. 265 –271.

[6] C. Yetis, T. Gou, S. Jafar, and A. Kayran, "On feasibility of interference alignment in MIMO interference networks," *IEEE Transactions on Signal Processing*, vol. 58, no. 9, pp. 4771 –4782, Sep. 2010.

[7] M. Razaviyayn, G. Lyubeznik, and Z. Luo, "On the degrees of freedom achievable through interference alignment in a MIMO interference channel," Apr. 2011, [Online]. Available: http://arxiv.org/abs/1104.0992.

[8] G. Bresler, D. Cartwright, and D. Tse, "Settling the feasibility of interference alignment for the MIMO interference channel: the symmetric square case," Apr. 2011, [Online]. Available: http://arxiv.org/abs/1104.0888.

[9] H. Jafarkhani, *Space-Time Coding: Theory and Practice*. Cambridge University Press, 2005.

[10] K. Gomadam, V. Cadambe, and S. Jafar, "A distributed numerical approach to interference alignment and applications to wireless interference networks," *IEEE Transactions on Information Theory*, vol. 57, no. 6, pp. 3309 –3322, Jun. 2011.

Capacity Bound of MOP-based Allocation with Packet Loss and Power Metrics in Satellite Communications Systems

Igor Bisio, *Member, IEEE,* Stefano Delucchi *Student Member, IEEE*, Fabio Lavagetto and Mario Marchese, *Senior Member, IEEE*

***Abstract*—The task of a capacity allocation policy is to determine the optimal quantity of capacity that has to be shared among the transmitting entities. In this work the allocation problem is modelled by the Multi Objective Programming (MOP) theory. In particular, an allocation criterion based on the *Tchebysheff* problem is proposed to find out a capacity allocation, among Earth Stations, representative of a compromise if Packet Loss Probability and Transmitted Power are taken into account as performance metrics. The paper also discusses the existence of a capacity allocation, called Capacity Bound, on which the performance converges independently of the overall capacity available C_{TOT}. A performance analysis, carried out through simulations and under different satellite channel conditions, is finally proposed to investigate the allocation criterion performance and to show the Capacity Bound existence.**

***Index Terms*—Satellite Communications, Multi-Objective Programming, *Tchebysheff* Problem-based Allocation, Capacity Bound, Performance Analysis.**

I. Introduction

THIS paper defines capacity allocation as a competitive problem where each entity (i.e., Earth Station) accessing the shared available capacity is "represented" by a group of functions called *objective functions*. Each of them needs to be optimised at cost of the others. These functions model physical quantities, such as Packet Loss Probability (PLP) and Transmitted Power (TP), as function of the capacity allocated to the entity. If the functions are in contrast each other the allocation must represent necessarily a compromise. Modelling capacity allocation as described allows using Multi-Objective Programming (MOP) theory, which defines the multi-objective optimisation problem and the set of Pareto Optimal Points (POPs) as introduced in [1]. Each POP is often referred to a vector analogue for optimal solutions because the optimal solution for MOP is not formally defined. Optimal capacity allocations are chosen among POPs. Even if each POP is optimal from Pareto viewpoint, is needed to choose one solution. A possibility, used in this paper, is the compromise solution [2], that selects a single POP minimising the distance, in the sense of *Tchebysheff* [3], with a reference goal point. In this paper, the solutions of the *Tchebysheff* problem has been evaluated by applying several weights combinations as well as different norms to investigate several compromises among the adopted metrics: PLP and TP. Moreover, starting from the definition of *Tchebysheff* problem and considering the specific analytical formulae of the *objective functions* adopted in this paper explicitly reported in Section IV, the existence of a Capacity Bound has been formally and experimentally proven. In more detail, under the considered conditions, the *Tchebysheff* problem provides the same solution (i.e., the allocation among entities does not change) even if the overall available capacity C_{TOT} tends to infinity. It means that the system performance does not change even if the resource availability, in terms of capacity expressed in [bps], significantly grows. Given a certain C_{TOT} and a given number of Earth Stations, the result allows considering the possibility to save capacity for other possible entities without performance detriment. The rest of the paper is organised as follows. The next section presents a brief survey of the state of the art about the capacity allocation for satellite and wireless communications systems. In Section III the MOP mathematical framework, used in this paper, is revised and the allocation criterion, modelled as the *Tchebysheff* problem, are presented. Section IV describes the analytical formulae employed as performance metrics in this work: PLP and TP. Section V shows that the compromise solution is independent of the overall available capacity C_{TOT}, if it significantly grows, by demonstrating the existence of the Capacity Bound under the considered conditions in this paper. Section VI presents the simulation results that confirm the existence of the mentioned Capacity Bound analytically found. Finally the Conclusions are drawn.

I. Bisio, S. Delucchi F. Lavagetto and M. Marchese are with the DITEN Department, University of Genoa, Genoa, Italy, e-mail: igor.bisio@unige.it, stefano.delucchi@unige.it, fabio.lavagetto@unige.it, mario.marchese@unige.it

II. Brief Survey of the State of the Art

Since the last decade the resource allocation for satellite and wireless communications systems is widely investigated. The most important resource considered by allocation algorithms is the capacity available, expressed in [bps], for data transmissions. The task of allocation algorithms concerned the maximisation of the capacity dedicated to each entity sharing the resource (i.e., the Earth Stations in this paper) aimed at improving the quality of communications.

Recently, algorithms that consider capacity allocation and TP, simultaneously, have been introduced. In general, the algorithms available in the literature can be divided in two families. The first family concerns the capacity maximization (in [bps]), provided to the overall communications system (i.e., to all entities) by allocating to each entity a certain quantity

of bandwidth, expressed in [Hz], and the power useful to carry out the communication process. The total amount of bandwidth and power assigned to the entities are constrained and the capacity is modelled as a function of bandwidth and power consumption according to the Hartley Shannon law. This approach can be found in [4] and [5].
The second family deals with the transmission power minimisation by allocating bandwidth (in [Hz]), and capacity (in [bps]). The TP by each entity, is analytically obtained by the Hartley Shannon Law. In such an approach the capacity is considered constrained over a given threshold to assure a certain level of communications quality. This approach can be found in [6] and in [7].
The main difference between the proposed method, based on the MOP theory and similarly presented in [1], and the families above surveyed concerns the optimisation criterion used for the resource allocation. In more detail, our proposal tries to optimise the value of two (or more, in general) metrics, simultaneously. The proposed MOP-based approach considers a single constrained control vector, the capacity allocated to each entity, and is explicitly aimed at optimising the Transmitted Power and a quality of service metric (the Packet Loss Probability in the case of this work), at the same time. On the contrary, the approaches found in the literature try to optimise a single metric (i.e., only one objective function), the capacity or the Transmitted Power, without explicit reference to quality of service parameters as done in this paper. Moreover, the proposed formulation allows showing the existence of a Capacity Bound that fixes the overall system performance and avoids possible capacity wasting.

III. The *Tchebysheff* Problem based Allocation

The model proposed in this paper is an extension of the proposals in [8], in [9] and [1] and is based on three main components: physical entities, virtual entities, and objective functions. [8] introduces the capacity allocation based on physical entities and objective functions; [9] opens the door to the concept of virtual entity by using more than one buffer for physical entity even if the term "virtual entity" is never mentioned. The main differences, introduced by this work, are the generalisation of the norm-based allocation method to find the POP compromise solution as suggested in [2], and, in particular, the proof of the existence of a Capacity Bound under the considered conditions of this paper detailed in Section V. As defined in [1] a physical entity is a device such as a satellite Earth Station. A virtual entity is a component within a physical device such as a single buffer-server. Each virtual entity is "represented" by a group of objective functions that model performance parameters such as, for instance, Packet Loss Probability and Transmitted Power. Capacity allocations are performed by a centralised decision maker, which split C_{TOT} among all physical entities and assigned portions of capacity to virtual entities in dependence on the objective functions value.

A. MOP-based Capacity Allocation over Satellite Communications Systems

In this section the capacity allocation problem is modelled as a MOP Problem previously formalised in [1] and here reported for the sake of completeness. The system is composed by Z physical entities; each physical entity is identified by $z \in [1, Z]$. Y_z is the number of virtual entities of the $z-th$ physical entity. Each virtual entity is identified by $y_z \in [1, Y_z]$. M_{y_z} is the number of objective functions for each virtual entity y_z. Each objective function, of a given $y_z - th$ virtual entity, is identified by the index $m \in [1, M_{y_z}]$. C_{y_z} is the capacity allocated to the virtual entity y of the physical entity z.

$$\mathbf{C} = (C_{1_1}, C_{2_1}, C_{3_1}, ..., C_{Y_1}, ..., C_{1_Z}, C_{2_Z}, C_{3_Z}, ..., C_{Y_Z}) \quad (1)$$

is the vector that contains the capacity allocated to each virtual entity. $C_z = \sum_{y=1}^{Y_z} C_{y_z}$ is the capacity allocated to physical entity z. $F_{m,y_z}(\mathbf{C})$ is the $m-th$ objective function, analytically defined in Section IV, of the $y-th$ virtual entity of the $z-th$ physical entity. The full set of objective functions is contained in the vector

$$\begin{aligned}\mathbf{F}(\mathbf{C}) = (&F_{1,1_1}(\mathbf{C}), ... \\ &F_{M_{1_1},1_1}(\mathbf{C}), ..., F_{1,Y_Z}(\mathbf{C}), ..., F_{M_{Y_Z},Y_Z}(\mathbf{C}))\end{aligned} \quad (2)$$

Given the definitions above and given C_{TOT} the available physical capacity, shared by all Z entities, the following constraint must hold:

$$\sum_{z=1}^{Z}\sum_{y=1}^{Y_z} C_{y_z} \leq C_{TOT} \quad (3)$$

Capacity allocation is defined as a MOP problem through (4), which must be solved under the constraint (3) that defines the feasibility region.

$$\begin{aligned}\mathbf{C}_{opt} = \Big(&C_{1_1,opt}, C_{2_1,opt}, .., C_{Y_1,opt}, .., \\ &C_{1_Z,opt}, C_{2_Z,opt}, .., C_{Y_Z,opt}\Big) = \arg\min_{\mathbf{C}} \mathbf{F}(\mathbf{C}); \\ &C_{y_z} \geq 0, \forall y_z \in [1, Y_z]. \forall z \in [1, Z]\end{aligned} \quad (4)$$

The set of solutions deriving from (4) is called POP set. In general, getting the overall POP set is not simple but the structure of the objective functions helps to take decision in some cases. For example, it is simple to prove that given the problem (4), subject to the constraint (3), if all objective functions are strongly decreasing [3], i.e. decreasing for all its variables and strictly decreasing for at least one function and one variable, then a solution $\mathbf{C}$ is a POP if and only if the solution is on the constraint boundary $\sum_{z=1}^{Z}\sum_{y=1}^{Y_z} C_{y_z} = C_{TOT}$. This is the case we have considered in [8] and [9]. It is also true that, given inequality constraint (3), if all objective functions are decreasing, all the points on the constraint boundary are POP solutions, but not all POP solutions necessarily belong to the constraint and also points for which $\sum_{z=1}^{Z}\sum_{y=1}^{Y_z} C_{y_z} < C_{TOT}$ can be POP solutions. The strongly decreasing assumption concerning the objective-function vector is quite typical because

common performance functions applied in telecommunication networks such as Packet Loss Probability, Packet Delay and Packet Jitter are quantities that decrease their values when the allocated capacity value increases. This is not true if also other important metrics are used: power, but also processing and computation effort. It is simple to prove that, given problem (4) and constraint (3), if at least one function is strongly increasing, i.e. increasing for all its variables and strictly increasing for at least one variable, all the points inside the feasibility region as well on the constraint boundary may be POP.

B. Tchebysheff Problem-based Allocation Criterion

The idea is to allocate capacity so that the value of each objective function is as close as possible to its ideal value. The set of ideal capacities (i.e. the ideal vector (5)) composed of the ideal decision variable vector elements $C_{y_z,id}^{F_{k,y_z}}$ for which F_{k,y_z} attains the optimum value, may be known having information about the features of the objective functions, as explained in the following. This definition of the ideal capacities set is not the only choice, e.g., if hard constraints on metrics were given, the ideal vector may contain the minimum capacity allocations so to assure these constraints.

$$\begin{aligned}\mathbf{C}_{id}^{F_{k,y_z}} = \Big(&C_{1_1,id}^{F_{k,y_z}}, C_{2_1,id}^{F_{k,y_z}}, ..., C_{Y_1,id}^{F_{k,y_z}}, ..., \\ &C_{1_Z,id}^{F_{k,y_z}}, C_{2_Z,id}^{F_{k,y_z}}, ..., C_{Y_Z,id}^{F_{k,y_z}}\Big) \\ &\forall k \in [1, M_{y_z}], \forall y_z \in [1, Y_z], \forall z \in [1, Z]\end{aligned} \tag{5}$$

Each element $C_{y_z,id}^{F_{k,y_z}}$ can assume a value between 0 and C_{TOT}, independently of any physical constraint and of the values of the other components of vector (5). It is called ideal (utopian) for this. For example, if a generic objective function is decreasing versus capacity, it is obvious that it is ideal allocating all the possible capacity C_{TOT}, while if it is increasing versus capacity, it is ideal allocating no capacity at all. The values of vector (5) are considered known in the remainder of the paper. Vector in (6) contains each objective function attaining its ideal value.

$$\begin{aligned}\mathbf{F}_{id} = \Big(&F_{1,1_1,id}\Big(\mathbf{C}_{id}^{F_{1,1_1}}\Big), .., F_{k,y_z,id}\Big(\mathbf{C}_{id}^{F_{k,y_z}}\Big), .., \\ &F_{M_{Y_Z},Y_Z,id}\Big(\mathbf{C}_{id}^{F_{M_{Y_Z},Y_Z}}\Big)\Big)\end{aligned} \tag{6}$$

The allocated optimal capacity based on the proposed criterion is reported in (7).

$$\begin{aligned}&\mathbf{C}_{all} = (C_{1_1,all}, C_{2_1,all}, ..., C_{Y_1,all}, ..., C_{1_Z,all}, C_{2_Z,all}, ..., \\ &C_{Y_Z,all}) = \arg \min_{\mathbf{C} \subset \mathbf{C}_{opt}} J_p(\mathbf{C})\end{aligned} \tag{7}$$

where

$$\begin{aligned}J_p(\mathbf{C}) = \Bigg(\sum_{z=1}^{Z} \sum_{y=1}^{Y_z} \sum_{k=1}^{M_{y_z}} w_{k,y_z} \Big| &F_{k,y_z}(\mathbf{C}^{F_{k,y_z}}) - \\ &+ F_{k,y_z,id}\Big(\mathbf{C}_{id}^{F_{k,y_z}}\Big)\Big|^p \Bigg)^{1/p}\end{aligned} \tag{8}$$

and $\sum_{k=1}^{M_{y_z}} w_{k,y_z} = 1$, $w_{k,y_z} \geq 0, \forall k \in [1, M_{y_z}]$, $\forall y_z \in [1, Y_z], \forall z \in [1, Z]$ so to assure the Pareto optimality of the solution as indicated in reference [3], page 98.

As extensively described in [2], the summation arguments in (8) can be considered in two ways: *i)* as transformations of the original objective functions; *ii)* as components of a distance function that minimizes the distance between the solution point and the ideal value, also called utopia point, in the criterion space. In practice, in this paper we minimise the distance (i.e., the norm) with respect to the utopia point, which gives origin to a POP solution [3] and is also known as Compromise Programming method. $J_p(\mathbf{C})$ is a function representing the generic norm, usually indicated with the symbol L_p [3], applied to calculate the distance from the ideal vector. In Section VI is reported a comparative performance analysis, carried out by varying norms and weights combinations, aimed at finding the better choice for the capacity allocation problem. The use of weights w_{k,y_z}, as well as different norms, allows allocating capacity to virtual entities by differentiating the importance of the performance metrics for different virtual entities up to neglecting one or more metrics, if necessary. This may be important to give more elasticity to capacity allocation also in dependence on the provided service (e.g., telephony, video-conferencing, audio/video streaming, web transactions) and on the provider/user requirements (e.g., capacity and energy costs, objective performance metrics versus P-QoS).

IV. The Objective Functions

In this paper each physical entity represents an Earth Station that transmits through a satellite channel. It is modelled as a single buffer (as a consequence, physical and virtual entities are not differentiated). Each considered entity is represented by two objective functions that are the Packet Loss Probability, shortly PLP, due to congestion ($F_{1,1_z} = P_{loss_z}(C_z)$) and the Transmitted Power, shortly TP, ($F_{2,1_z} = W_{tx_z}(C_z)$) and the constrain is defined by the amount of available capacity ($\sum_{z=1}^{Z} \sum_{y=1}^{Y_z} C_{y_z} \leq C_{TOT}$).

A. Packet Loss Probability Function

The PLP model used in this paper deals with Transmission Control Protocol (TCP) based traffic and is analytically reported in (9) as defined in [10]:

$$P_{loss_z}(C_z) = \frac{k_z \cdot N_z^2}{(\frac{R_z \cdot C_z \cdot rtt_z}{l} + Q_z)^2} \tag{9}$$

In this paper, the values of the variable reported in (9), applied in the performance analysis section, and the related meanings are: k_z=128/81 is a constant depending on TCP parameters, N_z =10 is the number of active TCP connection for the *z-th* station, Q_z is the buffer size, equal to 10 packets, for the *z-th* station. rtt is the the round trip time, is equal to 512 [ms], l =1500 [byte] is the TCP packet size and R_z and C_z are the code rate and the capacity allocated to the *z-th* station, respectively. Channel conditions vary over the time and, in this paper, the experienced Carrier to Noise ratio $\left(\frac{C}{N}\right)_z$ for each station represents the satellite channel status. Each Earth Satellite station is supposed to apply different code rates in dependence on the channel status. Code rates are assigned as in Table I. This hypothesis allows considering packet losses due to congestion because channel errors are made negligible by applying encoding. In (10) we rewrite the equation (9) in

TABLE I
APPLIED CODE RATES

$\left(\frac{C}{N}\right)_z$ [dB]	4.25-4.75	4.75-5.25	5.25-5.75	5.75-6.25	6.25-6.75
R_z	1/2	2/3	3/4	5/6	7/8

a simpler form. It will be useful in Section V for an easier mathematical tractability:

$$P_{loss_z}(C_z) = \frac{A_z}{(D_z \cdot C_z + Q_z)^2} \tag{10}$$

where $A_z(N_z) = k_z \cdot N_z^2$, $D_z(R_z) = \frac{Rc_z \cdot rtt}{l}$.

B. Transmitted Power Function

The TP of the *z-th* station is reported in (11):

$$W_{tx_z}(\alpha_z, C_z) = (2^{\frac{C_z}{B}} - 1) \cdot \alpha_z \tag{11}$$

α_z, called link constant in this paper, takes into account the parameters related to the link budget. In more detail, it contains the transmission antenna gain G_{T_z} of the *z-th* station, the receiver antenna gain on the satellite G_R (common for each station) both equal to 10^4, the Boltzman costant *k* equal to $1.38 \cdot 10^{-23} J \cdot K^{-1}$, the noise temperature *T* set to 290 [K], the bandwidth of the satellite channel *B*=1 [MHz] and the Free Space Loss (*FSL*) set equal to 10^{19} as defined in [11]. In practice, the coefficient α_z is:

$$\alpha_z = \frac{k \cdot T \cdot B \cdot FSL}{G_{T_z} \cdot G_R} \tag{12}$$

The Transmitted Power function is obtained by combining two equations: $C_z = B \cdot log_2\left(1 + \left(\frac{C}{N}\right)_z\right)$ the Hartley-Shannon law, and $\left(\frac{C}{N}\right)_z = \frac{G_{T_z} \cdot G_R \cdot W_{tx_z}}{k \cdot T \cdot B \cdot FSL}$ that represents the carrier to noise ratio [11].

V. THE CAPACITY BOUND OF THE COMPROMISE PROGRAMMING

In this paper we consider Z physical entities, a single virtual entity for each physical entity ($Y_z = 1 \; \forall z \in [1, Z]$) and two objective functions for each virtual entity ($k = 2 \; \forall y_z \in [1, Y_z], \forall z \in [1, Z]$). Considering the two objective functions previously introduced, the vector $\mathbf{F}(\mathbf{C})$, defined in (2), can be written as

$$\mathbf{F}(\mathbf{C}) = \Bigg(\frac{A_1}{D_1 C_1 + Q_1}, (2^{\frac{C_1}{B}} - 1)\alpha_1, ..., \frac{A_Z}{(D_Z C_Z + Q_Z)^2}, (2^{\frac{C_Z}{B}} - 1)\alpha_Z \Bigg) \tag{13}$$

According to (6) the utopia points for the employed objective function are $F_{1,1_z,id} = \frac{A_z}{(D_z C_{TOT} + Q_z)^2}$ and $F_{2,1_z,id} = 0$. Consequently, the function $J_p(\mathbf{C})$, representing the L_p norm applied, that needs to be minimised to obtain the POP solution of the so called Compromise Programming problem is, in practice, a function of the vector $\mathbf{C}$ and of the totally available capacity C_{TOT}:

$$J_p(\mathbf{C}, C_{TOT}) = \Bigg(\sum_{z=1}^{Z} \Big(\frac{A_z}{(D_z C_z + Q_z)^2} - + \frac{A_z}{(D_z C_{TOT} + Q_z)^2} \Big)^p + \Big((2^{C_z/B} - 1)\alpha_z \Big)^p \Bigg)^{1/p} \tag{14}$$

The aim of this section is to show that, given fixed channel conditions, if the overall capacity available for the entire communications system significantly grows, the POP solution provided by solving (7), considering $J_p(\mathbf{C}, C_{TOT})$ as defined in (14), will not significantly change tending, in the sense of a horizontal asymptote, to a quantity called Capacity Bound C^{bound}. From a formal viewpoint,

$$C^{bound} = \sum_{z=1}^{Z} C_z^{bound}, C^{bound} < C_{TOT} \tag{15}$$

The mentioned C^{bound} exist and is finished if $C_z^{bound} \; \forall z \in [1, Z]$ is a quantity independent of C_{TOT} when C_{TOT} tends to infinity. In practice, the following conditions must be satisfied:

Condition 1: The limits of the partial derivatives of the function $J_p(\mathbf{C}, C_{TOT})$ as C_{TOT} approaches to infinity are functions of the sole capacity vector $\mathbf{C}$:

$$\lim_{C_{TOT} \to \infty} \frac{\partial J_p(\mathbf{C}, C_{TOT})}{\partial C_z} = \partial J_{p,z}(\mathbf{C}), \forall z \in [1, Z] \tag{16}$$

Condition 2: C_z^{bound} must represent a coordinate of an equilibrium point:

$$C_z^{bound} = \{C_z \in [1, C_{TOT}) : \partial J_{p,z}(\mathbf{C}) = 0, \forall z \in [1, Z]\} \tag{17}$$

Condition 3: The Hessian matrix of the problem (7), $\mathbf{H}(\mathbf{C})$, must be positive-semidefinite:

$$\det\Big[\mathbf{H}(\mathbf{C})\Big] \geq 0, \forall C_z \in [0, C_{TOT}] \tag{18}$$

Obviously, the *Conditions 2* and *3* are related to the existence and uniqueness of the minimum of the functions $J_p(\mathbf{C}, C_{TOT})$ computed if $C_{TOT} \to \infty$.

In the specific case of this paper, considering the previously defined conditions, we firstly compute the gradient

$\nabla J_p(\mathbf{C}, C_{TOT})$ and we set it equal to zero to obtain the mentioned $J_p(\mathbf{C}, C_{TOT})$ minimum. In (19) is reported the $z-th$ component of the gradient vector:

$$\frac{\partial J_p(\mathbf{C}, C_{TOT})}{\partial C_z} = \Bigg(\Big(\frac{A_z}{(D_z C_z + Q_z)^2} - \frac{A_z}{(D_z C_{TOT} + Q_z)^2} \Big)^{p-1} \cdot \frac{-2A_z D_z}{(D_z C_z + Q_z)^3} + \Big(2^{C_z/B} - 1\Big)^{p-1} \cdot \frac{2^{C_z/B} ln(2) \alpha_z^p}{B} \Bigg) \cdot \Bigg(\sum_{z=1}^{Z} \Big(\frac{A_z}{(D_z C_z + Q_z)^2} - \frac{A_z}{(D_z C_{TOT} + Q_z)^2} \Big)^p + + \Big((2^{C_z/B} - 1)\alpha_z \Big)^p \Bigg)^{\frac{1}{p}-1} \tag{19}$$

As said about the $J_p(\mathbf{C}, C_{TOT})$ function, the $z-th$ component of the gradient is a function of $C_z, \forall z \in [1, Z]$, and C_{TOT}. In general, it means that the compromise solution is a function of C_{TOT}. If we consider a significant increasing of C_{TOT} (i.e., C_{TOT} tends to infinity) the contribute of the term $\frac{A_z}{(D_z C_{TOT} + Q_z)^2}$ decreases and tends to zero. Formally

$$\lim_{C_{TOT} \to \infty} \frac{\partial J_p(\mathbf{C}, C_{TOT})}{\partial C_z} = \Bigg(\Big(\frac{A_z}{(D_z C_z + Q_z)^2} \Big)^{p-1} \cdot \frac{-2A_z D_z}{(D_z C_z + Q_z)^3} + \Big(2^{C_z/B} - 1\Big)^{p-1} \cdot \frac{2^{C_z/B} ln(2) \alpha_z^p}{B} \Bigg) \cdot \Bigg(\sum_{z=1}^{Z} \Big(\frac{A_z}{(D_z C_z + Q_z)^2} \Big)^p + \Big((2^{C_z/B} - 1)\alpha_z \Big)^p \Bigg)^{\frac{1}{p}-1} \tag{20}$$

The expression defined in (20) shows that the solution of the equation $\nabla J_p(\mathbf{C}, C_{TOT}) = 0$ is independent of C_{TOT} (i.e., is constant with respect to C_{TOT}) if it significantly grows so satisfying *Condition 1*. Indeed, the expression found in (20) is $\partial J_{p,z}(\mathbf{C})$. In detail, the allocation that can be obtained by equation (20) depends only on the link constant, the protocol parameters and by the employed norm. Moreover, it is easy to proof that the *Conditions 2* and *3* can be easily satisfied. Obviously, the obtained C^{bound} represents a Capacity Bound, defined in (15), whose existence strictly depends on the conditions, in terms of objective functions, considered in this paper. From the practical viewpoint, a Service Provider may provide capacity allocations to the Z Earth Stations without employing the overall available capacity and may dedicate the rest of the capacity to other possible entities. It can be done without penalising the performance because the allocation represents a compromise (in the sense of [2]). On the other hand, the result allows designing the minimum amount of C_{TOT} needed to obtain a compromise solution among Z stations without capacity wasting.

VI. Performance Analysis

The scenario considered in this performance evaluation has been implemented through the *ns-2* simulator. It is composed by $Z = 2$ Earth Stations, that transmit TCP traffic over a common geostationary satellite channel. The overall duration of the simulation is 300 [s]. The allocation is done each 5 [s] (i.e., allocation period), and the channel condition experienced by each station, expressed by $\left(\frac{C}{N}\right)_z$, is randomly varied (by following a uniformly distributed probability density function of the values reported in Table I) and kept constant in each allocation period. The key concept of this paper is the Capacity Bound on which the compromise solution converges if the overall available capacity C_{TOT} significantly increases. As previously reported in Section V given the objective function that models the QoS, the Packet Loss Probability (PLP) $P_{loss_z}(C_z)$ (9), and the Transmitted Power (TP) $W_{tx_z}(\alpha_z, C_z)$, the compromise solution is not a function of the overall capacity C_{TOT} if it tends to infinity. In Fig. 1, the compromise solution is reported: it represents the capacity globally allocated to both the stations (i.e., the sum of the capacities allocated to the two stations) obtained by varying C_{TOT} in the interval $[1 - 10]$ [Mbps]. Four norms ($p = [1, 2, 3, 4]$) have been considered and both the metrics have been equally weighted ($w_{1,1_1} = w_{1,1_2} = 0.5$). The allocation of the overall available capacity has been reported as reference. The compromise solution stays on the constrain

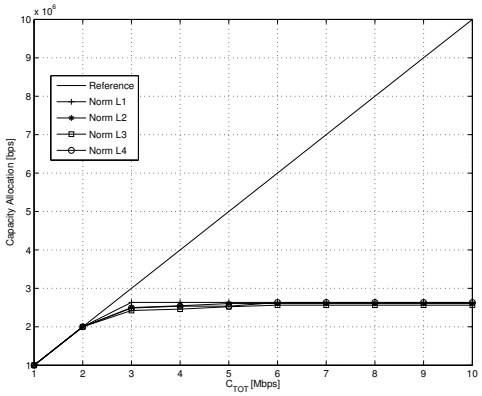

Fig. 1. Globally Allocated Capacity versus C_{TOT}.

if $C_{TOT} \leq 2$ [Mbps]. If $C_{TOT} > 2$ [Mbps] the compromise solution is constant around 2.6 [Mbps], for all the value of C_{TOT}. This is true for all the norms applied. It practically confirms the Capacity Bound whose existence has been discussed in Section V. The Capacity Bound has a significant impact on the performance. Fig. 2 shows that the PLP remains constant around 0.055. It is not far from the PLP level requested by many applications. In fact, as shown in Table III, the PLP level can be enhanced without impacting the TP significantly. The TP of a station is the second considered performance metric in this work coherently with Section IV. Its values are plotted in the Fig. 3. The TP is constantly lower than 0.1 [W] for each considered norm. This happens because the capacity allocated to each station, with the proposed method, is constant and both the objective functions, $F_{1,1_1}$ and $F_{1,1_2}$, are minimised during the allocation. If the allocations would follow the C_{TOT} behaviour the TP would grow exponentially. The proposed *Tchebysheff* Problem-based Allocation Criterion allows differentiating the solutions through weights applied

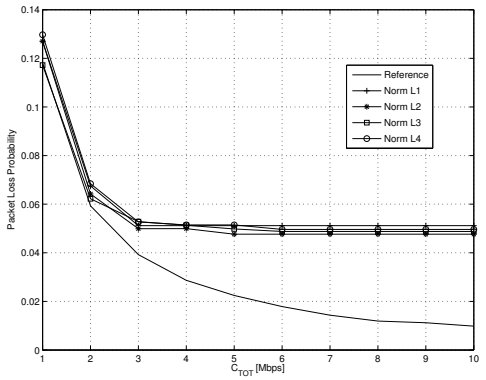

Fig. 2. Packet Loss Rate versus C_{TOT} variation.

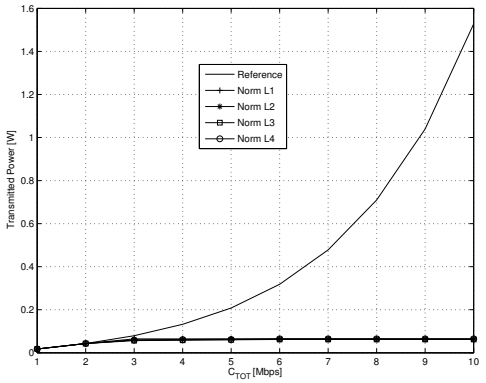

Fig. 3. Transmitted Power versus C_{TOT} variation.

to the objectives functions. Also the choice of a different norm to calculate the distance to the ideal point may modify the POP position. In the Table II the solutions in terms of capacity globally allocated to the two stations, over norms and weights variations are reported. For all the applied norms, the most capacity saving weights combination, among the case considered in this work, is $w_{1,1_1}$ = 0.1, $w_{1,1_2}$ = 0.9. This particular configuration assures also a reduction of power transmitted but also, at the same time, an increase of the packet loss rate, as reported in Table III and Table IV. Vice versa $w_{1,1_1}$ = 0.9, $w_{1,1_2}$ = 0.1 assures the minimum of the PLP but also the maximum TP, allocating the maximum of the capacity.

TABLE II
CAPACITY BOUND IN [BPS] VERSUS NORMS AND WEIGHTS VARIATIONS

$w_{1,1_1}$	0.9	0.75	0.5	0.25	0.1
$w_{1,1_2}$	0.1	0.25	0.5	0.75	0.9
Norm L_1	4805973	3698414	2763434	2035985	1328196
Norm L_2	3744290	3237478	2730666	2285021	1931127
Norm L_3	3368550	3012471	2686976	2453230	2202009
Norm L_4	3233109	2925090	2761250	2501290	2274099

VII. CONCLUSIONS

The work proposes a capacity allocation criterion based on the *Tchebysheff* problem representative of a compromise if Packet Loss Probability (PLP) and Transmitted Power (TP) are taken into account as performance metrics. Moreover, starting from the proposed *Tchebysheff* problem allocation and

TABLE III
PLP VERSUS NORMS AND WEIGHTS VARIATIONS

$w_{1,1_1}$	0.9	0.75	0.5	0.25	0.1
$w_{1,1_2}$	0.1	0.25	0.5	0.75	0.9
Norm L_1	0.02484	0.03425	0.051153	0.06913	0.10498
Norm L_2	0.03332	0.04113	0.047654	0.05864	0.07351
Norm L_3	0.03837	0.04373	0.048793	0.05839	0.06198
Norm L_4	0.04262	0.04507	0.049593	0.05329	0.06055

TABLE IV
TP IN [W] VERSUS NORMS AND WEIGHTS VARIATIONS

$w_{1,1_1}$	0.9	0.75	0.5	0.25	0.1
$w_{1,1_2}$	0.1	0.25	0.5	0.75	0.9
Norm L_1	0.17282	0.10504	0.06449	0.041283	0.02349
Norm L_2	0.10766	0.08353	0.06348	0.048509	0.038333
Norm L_3	0.08913	0.07446	0.06193	0.054092	0.045848
Norm L_4	0.08342	0.07080	0.06456	0.055427	0.048237

considering PLP and TP defined as in Section IV, the paper highlights the existence of a Capacity Bound on which the allocations converge. The bound is independent of the overall capacity available C_{TOT}. The proposed performance analysis shows the performance and the Capacity Bound existence. It allows concluding that the proposed method enables a significant capacity and TP saving and, simultaneously, a limited worsening of the PLP. Practically, a Service Provider may provide capacity allocations to Z Earth Stations without employing its overall available capacity and may dedicate the rest of it to other possible entities without penalising the overall performance and avoiding satellite capacity wasting.

REFERENCES

[1] I. Bisio and M. Marchese, "Power saving bandwidth allocation over geo satellite networks," *Communications Letters, IEEE*, vol. 16, no. 5, pp. 596 –599, may 2012.

[2] R. T. Marler and J. S. Arora, "Survey of multi-objective optimization methods for engineering," *Structural and Multidisciplinary Optimization*, vol. 26, no. 6, pp. 369 –395, apr. 2004.

[3] K. M. Miettinen, *Nonlinear Multiobjective Optimization*. Boston, USA: Kluwer Academic Publisher, 1998.

[4] D. Chen and J. Laneman, "Joint power and bandwidth allocation in multihop wireless networks," in *Wireless Communications and Networking Conference, 2008. WCNC 2008. IEEE*, 31 2008-april 3 2008, pp. 990 –995.

[5] X. Gong, S. Vorobyov, and C. Tellambura, "Joint bandwidth and power allocation with admission control in wireless multi-user networks with and without relaying," *Signal Processing, IEEE Transactions on*, vol. 59, no. 4, pp. 1801 –1813, april 2011.

[6] X. Wang and G. Giannakis, "Power-efficient resource allocation for time-division multiple access over fading channels," *Information Theory, IEEE Transactions on*, vol. 54, no. 3, pp. 1225 –1240, march 2008.

[7] W. Ho and Y.-C. Liang, "Efficient resource allocation for power minimization in mimo-ofdm downlink," in *Vehicular Technology Conference, 2008. VTC 2008-Fall. IEEE 68th*, sept. 2008, pp. 1 –5.

[8] I. Bisio and M. Marchese, "Minimum distance bandwidth allocation over space communications," *Communications Letters, IEEE*, vol. 11, no. 1, pp. 19 –21, jan. 2007.

[9] ——, "Packet loss and delay combined optimization for satellite channel bandwidth allocation controls," in *Communications, 2008. ICC '08. IEEE International Conference on*, may 2008, pp. 1905 –1909.

[10] ——, "Analytical expression and performance evaluation of tcp packet loss probability over geostationary satellite," *Communications Letters, IEEE*, vol. 8, no. 4, pp. 232 – 234, april 2004.

[11] L. J. Ippolito, *Satellite Communications System Engineering*. Chichester, UK: John Wiley & Sons Ltd, 2008.